J. Fluid Mech. (1992), *vol.* 234, *pp.* 553–581
Printed in Great Britain

Double-frequency forcing on spatially growing mixing layers

By OSAMU INOUE
Institute of Fluid Science, Tohoku University, 2-1-1 Katahira, Aoba-ku, Sendai 980, Japan

(Received 15 June 1990 and in revised form 16 July 1991)

Spatially growing mixing layers are simulated numerically using a two-dimensional vortex method. Special attention is paid to the effect of double-frequency forcing on the development of a mixing layer. Two different types of forcing are considered: superposition of a fundamental frequency (F) on one of its subharmonics (Case I), and superposition of two frequencies of a resonance type, $F \pm \Delta F$ (Case II). The effects of forcing amplitude and relative phase shift between the two forcing frequencies are also examined. Instantaneous plots of discrete vortices and various statistics up to the second-order moment are obtained to see the variation of coherent structures. Results show that the number of merging vortices and thus the growth of a mixing layer can be effectively controlled by double-frequency forcing if forcing frequencies, phase shifts and forcing amplitudes are suitably selected.

1. Introduction

Increasing attention has been given to forced mixing layers, because forcing may provide possible turbulence control. Experimental work has revealed that the growth of a mixing layer can be efficiently manipulated by imposing artificial disturbances on the flow. Zaman & Hussain (1980) imposed disturbances using sound from a loud speaker. The results showed that a reduction of turbulence intensity can occur under certain conditions of forcing. Ho & Huang (1982) imposed disturbances on a flow by controlling the flow rate. Their results showed that the number of merging vortices, and thus the spreading of a mixing layer, can be efficiently manipulated at low forcing frequencies, if the mixing layer is perturbed near a subharmonic of the response frequency. Oster & Wygnanski (1982) generated disturbances using a small vibrating flap installed downstream of the trailing edge of a splitter plate. They found that the growth of the mixing layer depends on both the amplitude and the frequency of the forced disturbances. Mehta *et al.* (1987) investigated the effect of initial periodic disturbances on a plane mixing layer. Disturbances are provided at the trailing edge of the splitter plate using an oscillating flap. They observed that the mixing-layer growth is enhanced when forcing frequency (f) is half the fundamental frequency (F) of the unforced mixing layer, but suppressed when f is twice F. All these experiments showed that the flow features of a mixing layer strongly depend on the forced disturbances. For a comprehensive review, readers are referred to Ho & Huerre (1984) and Wygnanski & Petersen (1987).

The study of the effects of double-frequency forcing on a turbulent mixing layer is important. Ho & Huang (1982) observed that the location at which vortex merging occurs coincides with the location at which a subharmonic frequency attains a

maximum amplitude. Therefore, vortex merging may be intimately associated with the existence of two frequencies: a fundamental frequency and a subharmonic. On the other hand, Weisbrot & Wygnanski (1988) observed, in a highly excited mixing layer, that the first harmonic frequency is predominant in the region where the growth of a mixing layer is enhanced (Region I in Oster & Wygnanski 1982). The formation of a significant subharmonic frequency was not observed even in region III where the growth of the mixing layer is resumed. Weisbrot & Wygnanski think that a resonance of the Kelly (1967) type may occur between the fundamental frequency and the first harmonic rather than between the fundamental and its subharmonic. Thus, it is not necessarily clear whether the presence of a subharmonic is a necessary condition for the vortex merging process (Wygnanski & Weisbrot 1988).

The use of multiple-frequency forcing may have the possibility of drastically changing the flow structures, as suggested by Wygnanski & Petersen (1987). Hussain & Husain (1989) observed in their experimental study of a single-stream mixing layer that, when the mixing layer is forced by two frequencies (the fundamental frequency and its first subharmonic), the growth of a velocity fluctuation (r.m.s. u') depends on the phase shift between the two frequencies. These observations also indicate the importance of the study of the effects of double-frequency forcing.

A two-dimensional numerical approach to forced mixing layers is reasonable because two-dimensionally forced mixing layers which are produced experimentally become more two-dimensional than the unforced mixing layers (Oster & Wygnanski 1982). Thus, two-dimensional computational work on forced mixing layers has been performed fairly extensively: for example, Riley & Metcalfe (1980) using a direct Navier–Stokes simulation of a time-developing flow, Mansour, Hussain & Buell (1988) using a direct Navier–Stokes simulation of a spatially growing flow, Inoue & Leonard (1987*a*, *b*) using a vortex simulation of spatially growing mixing layers, Jacobs & Pullin (1989) using a contour-dynamics simulation of a time-developing flow, and so on.

Computational works on multiple-frequency forced mixing layers are not abundant. In most simulations except for Mansour *et al.* (1988) and Inoue (1989), spatial periodicity was assumed in order to simplify the calculations, which consider a temporal evolution of the flow. Jacobs & Pullin (1989) found in their numerical simulation of time-developing flows that, when the fundamental frequency is combined with the first subharmonic frequency, the rolled-up vortices showed either pairing interaction or tearing interaction depending on whether the phase shift between the two frequencies is zero or $\frac{1}{2}\pi$. A similar dependence of the nature of vortex interaction on the phase shift between the fundamental frequency and its first subharmonic had been observed by Patnaik, Sherman & Corcos (1976) and by Riley & Metcalfe (1980). Wygnanski & Petersen (1987) claim that calculations based on the temporal evolution of the flow overemphasize the importance of the phase shift because temporal waves are non-dispersive.

This study is an extension to double-frequency forced cases of the work done by Inoue & Leonard (1987*a*, *b*) for single-frequency forced, spatially growing mixing layers. In vortex methods, convergence of a solution to an ultimate state as the number of vortices is increased is very difficult to show. It is not clear whether there even is convergence. However, Inoue & Leonard reproduced many of the flow features which have been observed experimentally. Statistics up to the second-order moment showed excellent agreement with experiments. Therefore, the model and the method used by Inoue & Leonard are expected to give valuable information about the dynamics of forced mixing layers. One of the goals of this study is to increase our

understanding of the effects of multiple-frequency forcing on the development and structure of a mixing layer. For this purpose, we use the same flow model as that used in the study of single-frequency forced mixing layers.

2. Mathematical formulation and numerical procedure

2.1. *Flow model and simulation parameters*

In Lagrangian simulations using the vortex method, unlike Eulerian simulations using the Navier–Stokes codes, the streamwise velocities of the two uniform flows, U_1 and U_2, are not specified as boundary conditions at $y = \pm\infty$. Instead, vortices existing in the computational domain determine U_1 and U_2 according to the Biot-Savart law. Therefore, the determination of the circulation of each discrete vortex and the use of a good flow model are important in the vortex method in order to create a flow field with the desired velocities U_1 and U_2. In this study, we use the following flow model and method to determine the circulation, because this model has been shown to work very well in the study of single-frequency forced mixing layers. For details, readers are referred to Inoue & Leonard (1986, 1987*a*).

First, an unbounded flow produced by an infinite row of discrete vortices with the same sign and the same strength which are moving along the x-axis with a constant velocity is considered. Let the circulation of each vortex be denoted by Γ, the fixed distance between the two neighbouring vortices by l, the constant velocity of translation of the row by U_c, and the velocities of the upper and lower flows far from the x-axis, by U_1 and U_2, respectively. Then the following relations are satisfied:

$$\Gamma = \Delta U l, \quad \Delta U = U_1 - U_2, \quad U_c = \tfrac{1}{2}(U_1 + U_2). \tag{1}$$

Next, let us suppose that at an initial instant, $t = 0$, vortices on the right ($x > 0$) are suddenly removed. At all subsequent times the vortices on the left ($x < 0$) are assumed to move along the x-axis with the convection velocity U_c. After reaching the origin ($x = 0$), each vortex at $x > 0$ is assumed to move under the influence of the potential field induced by individual vortices including the upstream ($x < 0$) vortices, in addition to the contribution of the convection velocity U_c. Our main interest lies in the motion of the discrete vortices on the right-hand side. To simulate a flow produced in a wind tunnel, the effect of walls which bound the mixing layer at $y = \pm L$ is taken into consideration. The effect of the walls is approximated by two rows of image vortices (figure 1). These image vortices have the opposite sense of circulation and half the strength of the real vortices. This ensures that the total circulation of the flow field remains at zero. Strictly speaking, by this approximation the normal velocities on the walls do not satisfy the wall condition: the normal velocity V on the walls was less than 1.6% of ΔU and the r.m.s. v' on the walls was less than 0.5% of ΔU. However, it has been confirmed that the simplified wall model adopted here produces no practical problems (Inoue & Leonard 1986, 1987*a*). The complex velocity potential, $\mathscr{f}$, which governs the flow development for N vortices, is given by

$$\mathscr{f} = U_c z + \mathrm{i}\sum_{n=1}^{N}\frac{\Gamma}{2\pi}\log(z-z_n) - \mathrm{i}\sum_{n=1}^{N}\frac{\Gamma}{4\pi}\log(z-z_{u,n}) - \mathrm{i}\sum_{n=1}^{N}\frac{\Gamma}{4\pi}\log(z-z_{l,n}) \tag{2}$$

where $z = x + \mathrm{i}y$, and the subscripts u and l denote the upper and lower image vortices, respectively. The velocity components u in the x-direction and v in the y-direction are given by

$$u - \mathrm{i}v = \partial\mathscr{f}/\partial z. \tag{3}$$

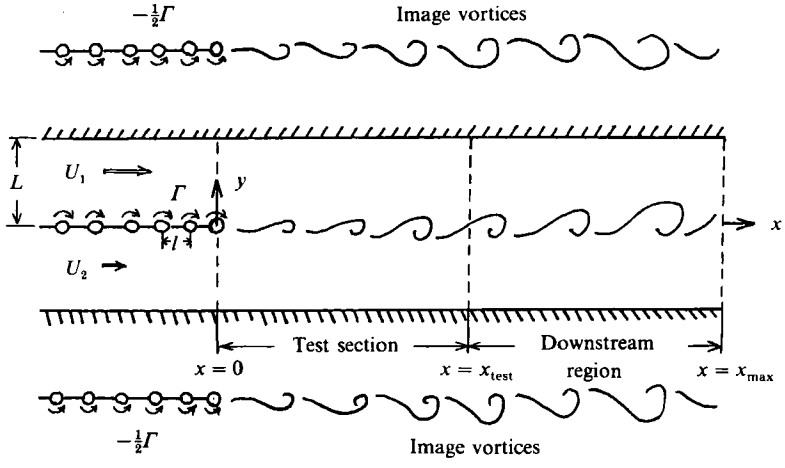

FIGURE 1. Schematic of flow model

The time development of an individual vortex is determined from the relations

$$\frac{\mathrm{d}x_n}{\mathrm{d}t} = u_n, \quad \frac{\mathrm{d}y_n}{\mathrm{d}t} = v_n. \tag{4}$$

As is well known, the numerical algorithm employed here requires evaluation of order N^2 terms per time step and therefore is time consuming for large N. To save computation time, we assume a test section in which reliable results are expected to be defined as $0 < x < x_{\text{test}}$, and vortices far downstream ($x \geqslant x_{\max} > x_{\text{test}}$) of the test section are deleted. This treatment ensures that the maximum number of discrete vortices in the computational domain is within a certain limit, and thus allows a calculation to be made for a period long enough that statistics can be measured. On the other hand, the deletion of vortices from the computational domain might cause the mixing layer to be perturbed and thus the desirable forcing described later in this section is polluted at the origin. Buell & Huerre (1988) found in their Navier–Stokes simulation of a spatially growing mixing layer that the exit boundary condition causes global potential fluctuations which interact with the inflow boundary and create small-amplitude noise at the inlet. As seen in the next section, however, the results in the present vortex simulation are not affected significantly by the feedback mechanism. The first-order Euler scheme is employed for time-integration.

In this simulation, as well as in the previous study, length- and timescales are arbitrary, because in a mixing layer there is no characteristic lengthscale. As will be seen in §3, however, statistic quantities are presented in conventional non-dimensional forms. The simulation parameters were prescribed as follows:

$$\begin{gathered} L = 50, \quad x_{\text{test}} = 250, \quad x_{\max} = 500, \\ \text{time step:} \quad \delta t = 0.1, \\ \text{convection velocity:} \quad U_c = 3.2, \\ \text{velocity ratio:} \quad r\,(\equiv U_2/U_1) = 0.6. \end{gathered} \tag{5}$$

It has been confirmed, by comparing flow features between the two cases of $\delta t = 0.1$ and 0.05, that the time step $\delta t = 0.1$ is sufficiently short. The distance between two neighbouring vortices upstream of the origin was prescribed to be $l = U_c\,\delta t\,(=0.32)$. Therefore, one vortex is shed at each time step from the origin. With these values,

we obtain $U_1 = 4.0$, $U_2 = 2.4$, $\Delta U = 1.6$ and $\Gamma = 0.512$ from equation (1). In actual computations, however, vortices far downstream are deleted from the computational domain, and hence the infinite sheet of vortices which set up the velocity jump does not exist: equation (1) does not hold. As mentioned before, in the vortex method U_1 and U_2, and thus ΔU, are determined after computation has finished. Our flow model with the parameters described by (5) and also with Γ estimated by (1) gives $4.0 \leqslant U_1 \leqslant 4.02$, $2.4 \leqslant U_2 \leqslant 2.41$ and $1.59 \leqslant \Delta U \leqslant 1.62$ in the test section $0 \leqslant x \leqslant 250$.

Forcing is applied such that each new discrete vortex appears at a position

$$x = 0, \quad y = y_f(t), \tag{6}$$

where y_f is assumed to be a sinusoidal function of time. This flow situation may be realized by a vibrating flap at the end of a splitter plate. As our main interest lies in double-frequency forcing, $y_f(t)$ is assumed to be of the form

$$y_f = A_1 \sin(2\pi f_1 t) + A_2 \sin(2\pi f_2 t + \beta). \tag{7}$$

The parameters prescribed for forcing are as follows:

$$\begin{aligned}
&\text{forcing amplitude:} \quad A_1 = 0.5 U_c\, \delta t \text{ (fixed)},\\
&\text{amplitude ratio:} \quad a\,(\equiv A_2/A_1) = 0.05,\ 0.2,\ 0.5,\ 1.0,\ 2.0\\
&\text{phase angles:} \quad \beta = 0\text{–}\pi,\\
&\text{forcing frequencies:}\\
&\qquad \text{Case I: } f_1 = F \text{ (fixed)}, \quad f_2 = \tfrac{1}{2}F,\ \tfrac{1}{3}F,\ \tfrac{1}{4}F,\\
&\qquad \text{Case II: } f_1 = F + \Delta F, \quad f_2 = F - \Delta F, \quad \Delta F = F/n \quad (n = 4,\ 6,\ 8).
\end{aligned} \tag{8}$$

The forcing given by (6) and (7) with $A_1 = 0.5 U_c\, \delta t$ is different from that in Inoue & Leonard (1987*a*, *b*) where, instead of y_f, velocity disturbance v_f was prescribed at the origin by the same sinusoidal form as (7) with $A_1 = 0.5 U_c$. It has been confirmed, however, that the differences between calculated results are sufficiently small, and no qualitative flow features are altered at all between the two forcing methods. The fundamental frequency F was determined as follows. In the experiments of Oster & Wygnanski (1982) the fundamental frequency F of the unforced mixing layer with $r = 0.6$ satisfied the following relation near the trailing edge of a splitter plate:

$$\frac{F\theta_i}{U_1 + U_2} \approx 0.02. \tag{9}$$

In our calculation $U_1 + U_2 = 2U_c = 6.4$, and the momentum thickness θ_i obtained near the start of linear growth of the unforced mixing layer is approximately equal to 0.4, as will be seen later in figure 3. Therefore, from the above relation (9), we prescribed the fundamental frequency as $F \approx 0.32$.

The magnitude of forcing amplitude A_1 is selected to be $0.5 U_c\, \delta t$ because, in the previous study of a single-frequency forced mixing layer, with a value of $A_1 \geqslant 0.5 U_c\, \delta t$ the characteristic flow features such as the double-peaked profile of r.m.s. u' and the negative Reynolds shear stress, both in region II, were captured very clearly (see figure 14 in Inoue & Leonard 1987*a*). The relative magnitude of the present forcing amplitude to experiments or other computations may be estimated as follows. In the experiments of Ho & Huang (1982) the r.m.s. forcing amplitude of velocity disturbances at the higher-speed side was less than $0.001 U_c$ in most cases except for collective interaction which required an amplitude larger than $0.02 U_c$. In the Navier–Stokes simulation of Mansour *et al.* (1988), the forcing amplitude was $0.005 \Delta U$ which was much larger than the amplitude of noise causes by the feedback

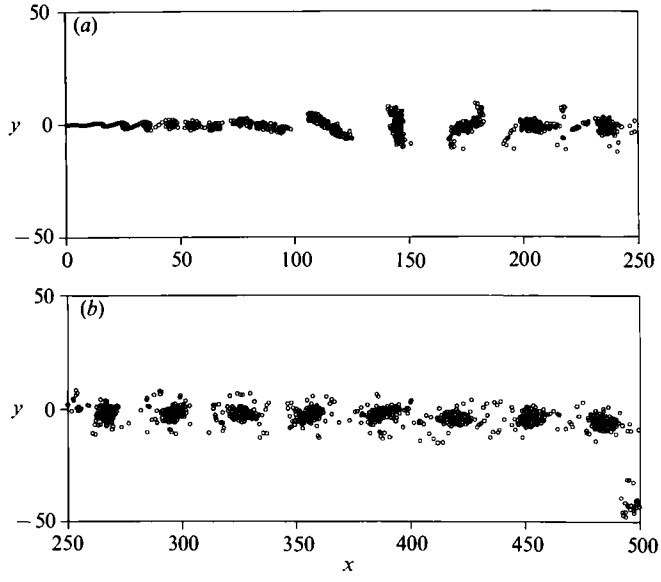

FIGURE 2. Flows at $t = 200$ when measurement of velocity fields were started. Case I: $f = F + \frac{1}{3}F$, $\beta = \frac{1}{2}\pi$. (*a*) $0 \leqslant x \leqslant x_{\text{test}}\,(=250)$, (*b*) $x_{\text{test}} \leqslant x \leqslant x_{\max}\,(=500)$.

mechanism from the exit boundary. In the present computation, the forcing amplitude of velocity disturbances may be estimated roughly as $(\mathrm{d}y_f/\mathrm{d}t)_{\max} = 2\pi f_1 A_1 \approx \pi F U_c \delta t \approx 0.1 U_c\,(=0.2\Delta U)$. Therefore, the present forcing amplitude may be larger than those of Ho & Huang and Mansour *et al.* Oster & Wygnanski (1982) used a vibrating flap. In their experiments, $f = 30$–60 Hz, $A_1 = 0$–2.0 mm and $\Delta U = 5.4$ m/s when $r = 0.6$. Therefore, if we introduce a non-dimensional forcing amplitude A_c which is defined as $A_c = A_1 f/\Delta U$, then A_c is estimated to be less than 2.2×10^{-2} in Oster & Wygnanski. In the present computation, $A_1 = 0.5 U_c \delta t = 0.16$, $f \leqslant F = 0.32$ and $\Delta U = 1.6$, and therefore $A_c \leqslant 3.2 \times 10^{-2}$ which is comparable to the value of Oster & Wygnanski.

At the initial stage of development, vortices leaving the origin roll up into concentrated swirls. These swirls are convected downstream with a velocity approximately equal to U_c. After sufficient time, it appears that the state of the mixing layer in the test section is independent of the effect of the initial roll-up. In our calculation, the mixing layer was well developed in the test section, $0 \leqslant x \leqslant 250$, by the time $t = 200$ when measurement of velocity fields were started. As an example of flow states at $t = 200$, figure 2 shows a flow for a double-frequency forced case when the fundamental frequency F is combined with a subharmonic $\frac{1}{3}F$ ($f_1 = F, f_2 = \frac{1}{3}F$ in Case I). Figure 2(*a*) is for the flow in the test section while figure 2(*b*) is for the flow in the downstream region. We can see from figure 2(*b*) that most of the initial swirls have passed through the location $x = x_{\max}$, and only a few remaining vortices of the initial swirls can be seen in the lower right-hand corner. In this simulation, as in the previous study of single-frequency forced cases, velocities are measured at twelve x stations from 20 to 240, and 51 y points from -20 to 20 at each x-station. The mean flow quantities and statistics are obtained by averaging instantaneous values over the period $200 \leqslant t \leqslant 1400$, which gives 12000 sampling data points for averaging purpose. A much longer calculation over $200 \leqslant t \leqslant 11000$ confirms that the shorter averaging time is enough to obtain accurate values of statistics up to the second-order such as the Reynolds shear stress $-\overline{u'v'}$ (Inoue & Leonard 1986).

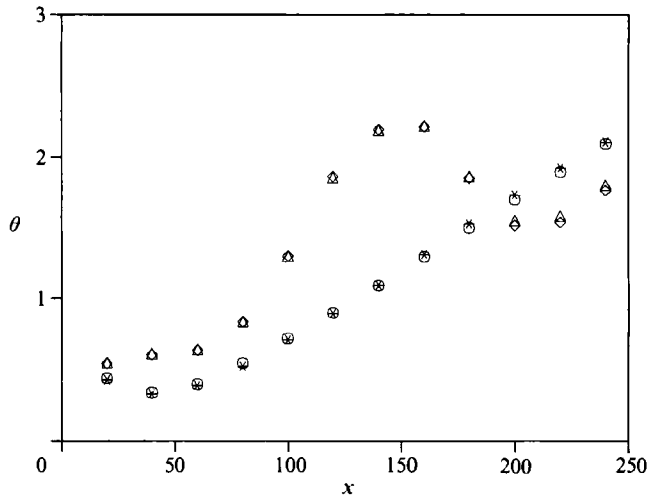

FIGURE 3. Momentum thickness distributions for unforced and double-frequency forced flows, $r = 0.6$. $f = 0$: ○, unforced flow with $x_{max} = 500$; *, unforced flow with $x_{max} = 650$. $f = F + \frac{1}{3}F$, $a = 1.0$, $\beta = \frac{1}{2}\pi$, △, forced flow with $x_{max} = 500$; ◇, forced flow with $x_{max} = 650$.

2.2. *Preliminary tests*

A number of preliminary tests on the simulation parameters prescribed in the previous section had been performed to verify that the spatial and temporal discretizations are adequate, and they are summarized in Inoue & Leonard (1986). In this study, however, we made additional tests on x_{max} in order to confirm that the flow features are not affected by x_{max} and also by the feedback mechanism mentioned in the previous section.

To test the effect of x_{max}, calculated flow features with the values 500 and 650 were compared. With $x_{max} = 650$, the downstream region is 60% elongated from $250 \leqslant x \leqslant 500$ to $250 \leqslant x \leqslant 650$. Comparisons were made both for unforced and forced flows. A double-frequency forced flow in Case I with $f_1 = F, f_2 = \frac{1}{3}F, \beta = \frac{1}{2}\pi$ was selected as a sensitive test of a forced case because, as we will see later in §3.2.2, this flow is unstable to irregular disturbances and the vortex merging pattern is changed by the introduction of irregular disturbances from the simultaneous merging of vortices in sets of three to other patterns shown in figure 16. In other words, if feedback disturbances are strong enough, the simultaneous merging pattern of sets of three vortices should not appear.

Momentum thickness distributions are presented in figure 3. (See equation (10) in §3.1 for the definition of the momentum thickness.) Velocity measurements for the case of $x_{max} = 650$ were made over $300 \leqslant t \leqslant 1500$, because for this case the initial swirls have not passed through the downstream boundary $x = x_{max}$ by $t = 200$. As seen from figure 3, both for the unforced and double-frequency forced flows the differences of momentum thickness distributions between $x_{max} = 500$ and 650 are negligibly small. Similar results are obtained for the other statistic quantities up to the second order. Instantaneous plots of discrete vortices for $x_{max} = 650$ are presented in figure 4. As the characteristic features of these flows are discussed in detail in §3, here we just point out that there are no noticeable differences observed between $x_{max} = 500$ and 650. In particular, we mention that the simultaneous merging pattern of every three vortices in the double-frequency forced flow (figure 4*b*) appears in both cases (see figure 16*b* for $x_{max} = 500$). From these results we may

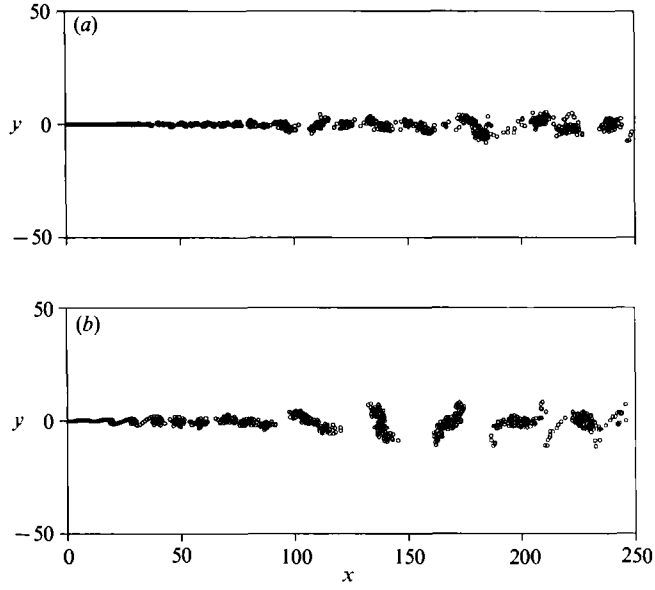

FIGURE 4. Instantaneous plots of discrete vortices at $t = 1500$: (*a*) unforced flow with $x_{max} = 650$, (*b*) double-frequency forced flow with $x_{max} = 650$. Case I: $f_1 = F$, $f_2 = \frac{1}{3}F$, $\beta = \frac{1}{2}\pi$, $a = 1.0$.

say that the prescribed downstream distance, $x_{max} = 500$, is sufficient to analyse flow fields accurately, and the flow features calculated with $x_{max} = 500$ are not affected significantly by the feedback mechanism mentioned in the previous section.

3. Results and discussion

3.1. *Single-frequency forced flows*

Before discussing the effect of double-frequency forcing, we briefly review the flow features of single-frequency forced mixing layers.

A shear layer emanating from the origin rolls up to form discrete vortices. Each rolled-up vortex then merges with other vortices and become larger. This merging process (often called the vortex pairing process) repeats with increasing downstream distance. Without forcing, the merging process occurs randomly in time and space, and as a result a time-averaged unforced mixing layer shows linear growth with increasing downstream distance. The calculated distributions of momentum thickness in the case of single-frequency forced mixing layer are presented in figure 5. For comparison, the distribution of momentum thickness for the unforced flow is also presented in the figure. The momentum thickness θ is defined as

$$\theta = \int \left\{ \frac{U-U_2}{U_1-U_2} \left(1 - \frac{U-U_2}{U_1-U_2} \right) \right\} \mathrm{d}y. \tag{10}$$

As seen clearly from the case of $f = \frac{1}{2}F$ in figure 5, the growth of a single-frequency forced mixing layer is characterized by three distinct subregions (Wygnanski & Petersen 1987): two growth regions (regions I and III in Wygnanski & Petersen) separated by one saturation region (region II). In region II no vortex merging is observed, and the profile of r.m.s. u' is double-peaked, and the Reynolds shear stress, $-\overline{u'v'}$, becomes negative across the mixing layer, indicating the occurrence of contra-gradient diffusion. These characteristic features of statistics are in excellent

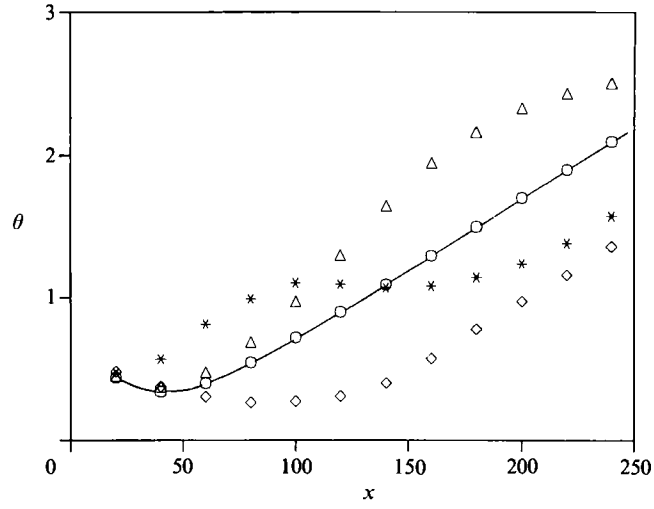

FIGURE 5. Effect of single-frequency forcing on momentum thickness. $r = 0.6$, $A_1 = 0.5U_c\,\delta t$. –○–, $f = 0$; *, $f = \frac{1}{2}F$; △, $f = \frac{1}{4}F$; ◇, $f = 2F$.

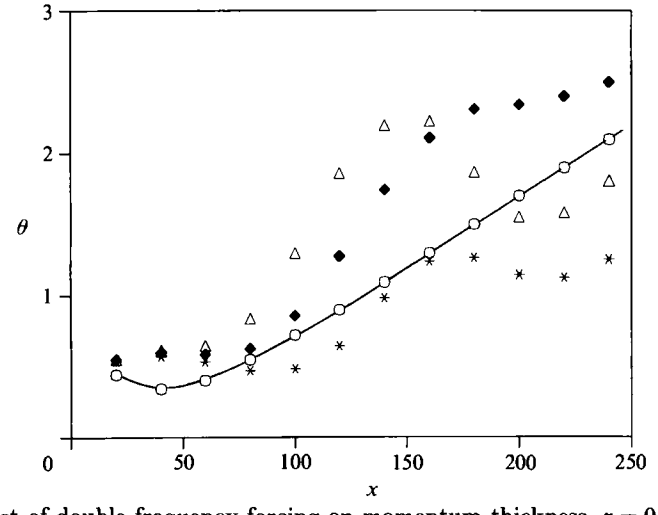

FIGURE 6. Effect of double-frequency forcing on momentum thickness. $r = 0.6$, $a = 1.0$. Case I. –○–, $f = 0$; *, $f = F + \frac{1}{2}F$, $\beta = 0$; △, $f = F + \frac{1}{3}F$, $\beta = \frac{1}{2}\pi$; ◆, $f = F + \frac{1}{4}F$, $\beta = 0$.

agreements with the experimental observation by Oster & Wygnanski (Inoue & Leonard 1987*a*, *b*). With decreasing forcing frequency, the length of region I increases; only region I can be seen for the case of $f = \frac{1}{4}F$ in figure 5. With increasing forcing frequency, the length of region I decreases, and for sufficiently high forcing frequencies region I does not appear; the mixing layer starts with the saturation region as seen in the case of $f = 2F$ in figure 5.

3.2. *Double-frequency forced flows (Case I)*

3.2.1. *Effect of forcing frequency*

A mixing layer forced by two frequencies behaves quite differently. Distributions of momentum thickness are presented in figure 6 where the fundamental frequency F is combined with its subharmonics $\frac{1}{2}F$ (the first subharmonic), $\frac{1}{3}F$, and $\frac{1}{4}F$ (the

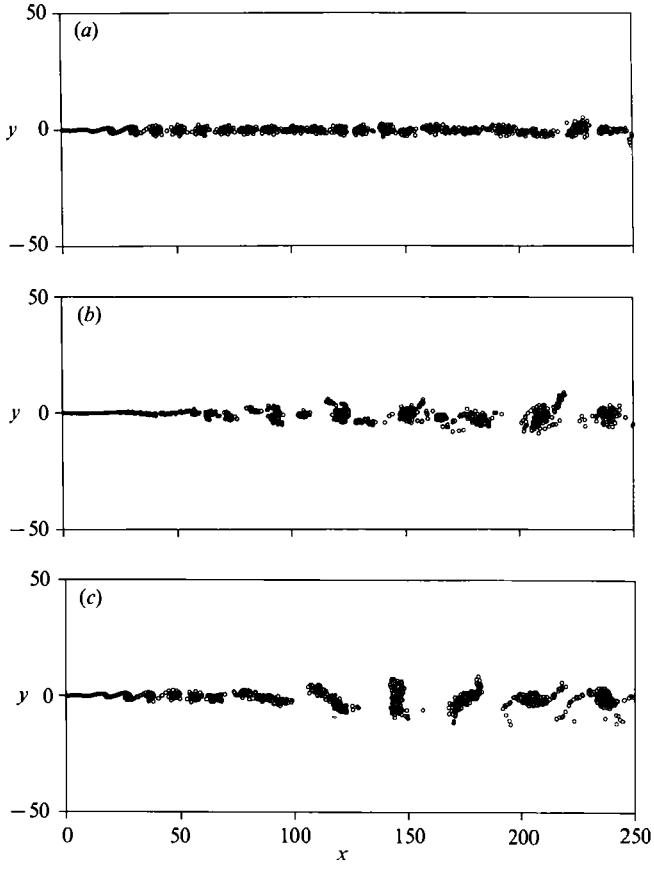

FIGURE 7. Effect of a subharmonic frequency combined with F on vortex motion at $t = 1400$, $r = 0.6$. (a) $f = F$, (b) $f = \frac{1}{3}F$, (c) $f = F + \frac{1}{3}F$, $\beta = \frac{1}{2}\pi$, $a = 1.0$ (Case I).

second subharmonic), respectively. In the figure, for simplicity, the expression $f = f_1 + f_2$ denotes the case $y_f = A_1 \sin(2\pi f_1 t) + A_2 \sin(2\pi f_2 t + \beta)$. As an example of double-frequency forced mixing layers presented in figure 6, an instantaneous plot of discrete vortices and a momentum thickness distribution for a case of $f = F + \frac{1}{3}F$ are shown, respectively, in figures 7 and 8. For comparison, the corresponding distributions of single-frequency forced cases with $f = F$ and $\frac{1}{3}F$ are also shown in the figures. When the fundamental frequency is combined with a subharmonic frequency, the fundamental frequency dominates the roll-up process immediately downstream of the origin, and the momentum thickness in this region is close to that of a single-frequency forced flow with $f = F$. This is clearly seen from figures 7 and 8, where both instantaneous plots of discrete vortices and momentum thickness distribution show that the roll-up process downstream of the origin ($0 \leqslant x \leqslant 50$) for the case $f = F + \frac{1}{3}F$ is close to that for $f = F$. The rolled-up vortices then tend to merge regularly and the momentum thickness downstream of the roll-up region increases (figure 6). The number of merging vortices in this region depends on the subharmonic frequency which is combined with the fundamental frequency; that is, sets of two vortices merge regularly when $f = F + \frac{1}{2}F$, sets of three when $f = F + \frac{1}{3}F$, and sets of four when $f = F + \frac{1}{4}F$. For an example of multiple-vortex merging, time developments of forced mixing layers when $f = F + \frac{1}{3}F$ and $F + \frac{1}{4}F$ are presented, respectively, in figures 9 and 10. In the figures, arrows indicate a merging process of a set of vortices. New vortices

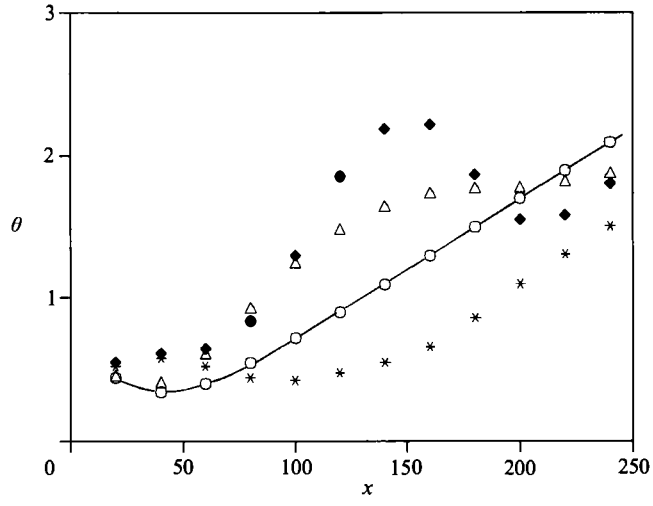

FIGURE 8. Effect of a subharmonic frequency combined with F on momentum thickness, $r = 0.6$. –○–, $f = 0$; *, $f = F$; △, $f = \frac{1}{3}F$; ◆, $f = F + \frac{1}{3}F$.

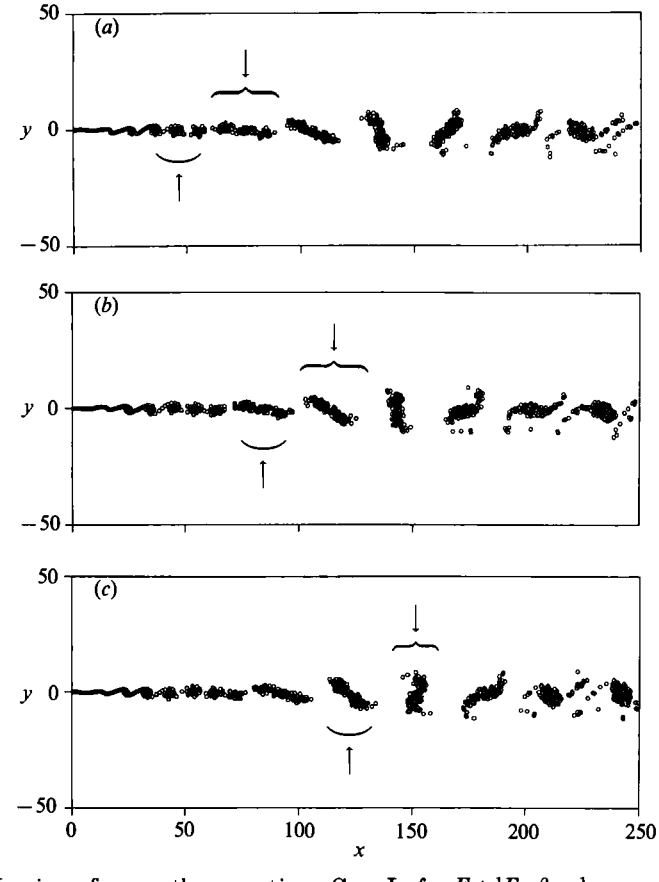

FIGURE 9. Merging of every three vortices. Case I: $f = F + \frac{1}{3}F$, $\beta = \frac{1}{2}\pi$, a = 1.0. (*a*) $t = 1406$, (*b*) $t = 1418$, (*c*) $t = 1430$.

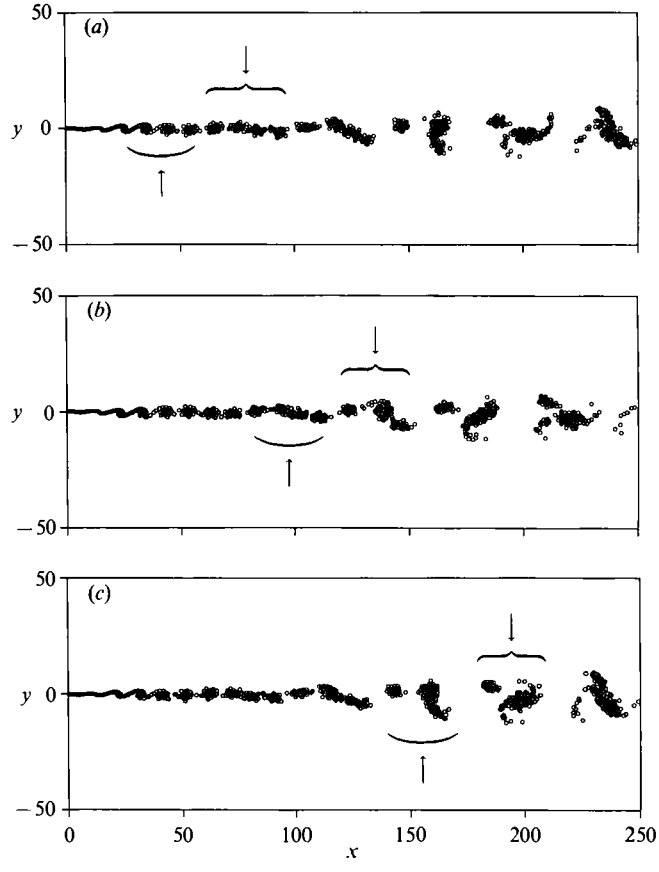

FIGURE 10. Merging of every four vortices. Case I: $f = F + \frac{1}{4}F$, $\beta = 0$, $a = 1.0$. (*a*) $t = 1412$, (*b*) $t = 1430$, (*c*) $t = 1448$.

which are produced by multiple-vortex merging lead a saturation region where vortex merging is inhibited. As seen from figure 6, the thickness ratio before and after multiple vortex merging is about 2 for $f = F + \frac{1}{2}F$, 3 for $f = F + \frac{1}{3}F$ and 4 for $f = F + \frac{1}{4}F$, though a pretty large overshoot can be seen for $f = F + \frac{1}{3}F$ with $\beta = \frac{1}{2}\pi$ (see also figure 13 below). Downstream of the saturation region, the mixing layer recovers its growth. The calculated flow features discussed above are quite similar to those observed experimentally by Ho & Huang (1982). Jacobs & Pullin (1989) observed in their contour-dynamics simulation of a time-developing shear layer that three vortices merge simultaneously when the fundamental frequency F is combined with a subharmonic $\frac{1}{3}F$.

The effect on the Reynolds stresses of combining two frequencies is shown in figures 11 and 12 for $f = F + \frac{1}{2}F$. The velocities are made dimensionless by ΔU. The profiles of r.m.s. u' in figure 11 (*a*) show three peaks at $x = 140$ where two merging vortices are nearly laterally aligned, in accordance with the observation in Mode II of Ho & Huang, as shown in figure 11 (*b*). As in the cases of single-frequency forced flows, the profiles of the Reynolds shear stress, $-\overline{u'v'}$, in figure 12 show the occurrence of contra-gradient diffusion in a region where the growth of the mixing layer is suppressed. The three-peaked profile of r.m.s. u' and the negative Reynolds shear stress are observed also for $f = F + \frac{1}{3}F$ and $f = F + \frac{1}{4}F$.

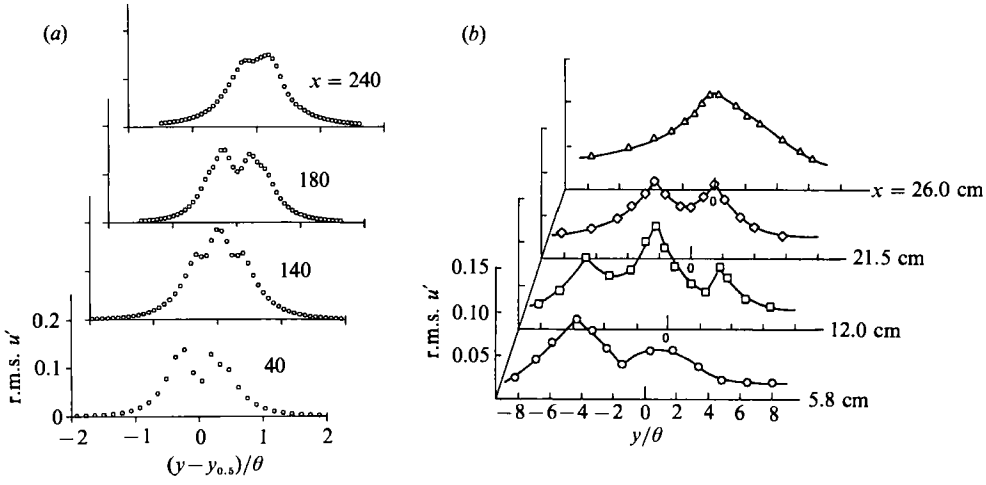

FIGURE 11. Profiles of r.m.s. u'. (*a*) Computational result for Case I: $f = F + \frac{1}{2}F$, $\beta = 0$, $a = 1.0$. (*b*) Experimental result for Mode II by Ho & Huang (1982).

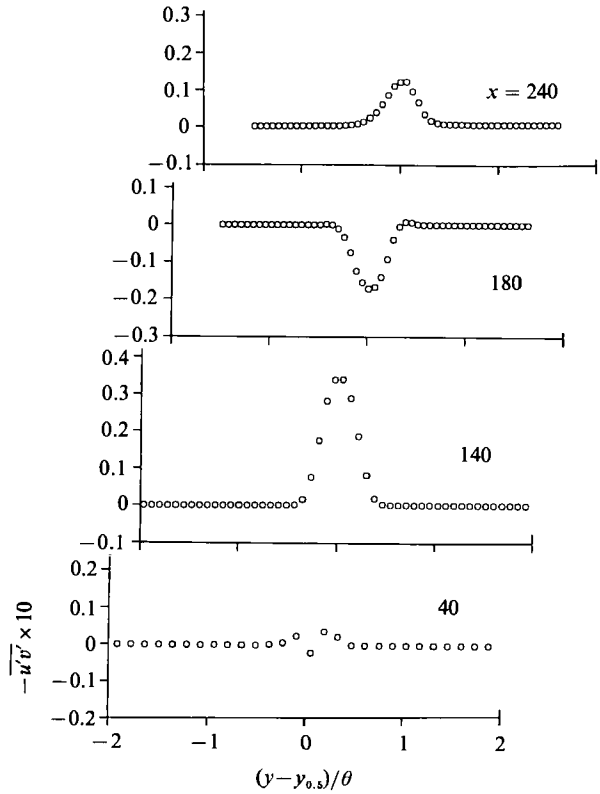

FIGURE 12. Profiles of $-\overline{u'v'}$. Case I: $f = F + \frac{1}{2}F$, $\beta = 0$, $a = 1.0$.

3.2.2. *Effect of phase shift*

The ranges over which the relative phase angle β varies are π when $f = F + \frac{1}{2}F$, $\frac{2}{3}\pi$ when $f = F + \frac{1}{3}F$, and $\frac{1}{2}\pi$ when $f = F + \frac{1}{4}F$. With these phase ranges in mind, the effect of β on the flow features is examined. The amplitude ratio a is fixed to be 1.0 in this

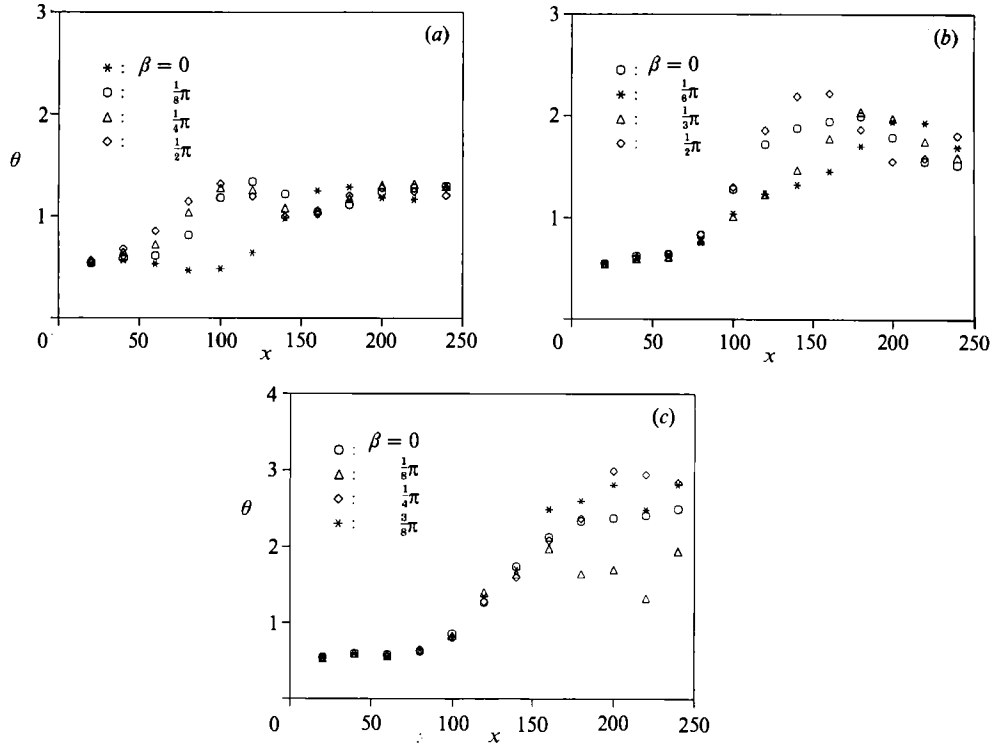

FIGURE 13. Effect of phase shift on momentum thickness. Case I: (*a*) $f = F + \frac{1}{2}F$, (*b*) $f = F + \frac{1}{3}F$, (*c*) $f = F + \frac{1}{4}F$.

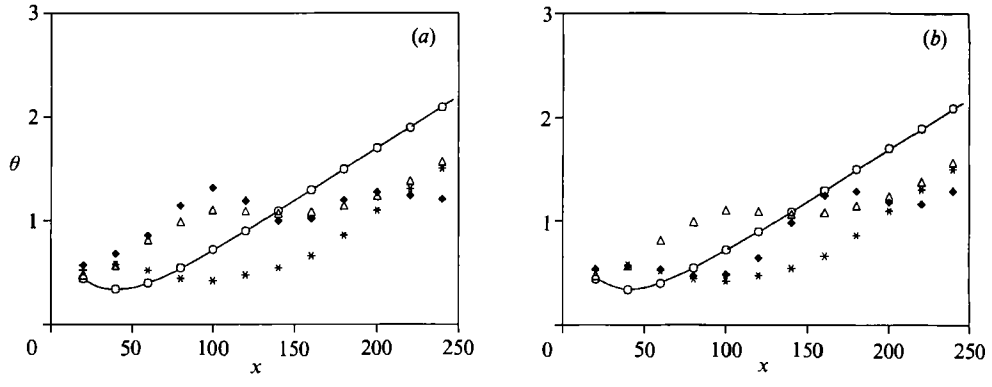

FIGURE 14. Difference of the mixing-layer growth between the two modes when $f = F + \frac{1}{2}F$ in Case I, $r = 0.6$, $a = 1.0$. (*a*) Mode I ($\beta = \frac{1}{2}\pi$), (*b*) Mode II ($\beta = 0$). –○–, $f = 0$, *, $f = F$; △, $f = \frac{1}{2}F$; ◆, $f = F + \frac{1}{2}F$.

section. Dependence of momentum thickness distributions on β is presented in figure 13 for $f = F + \frac{1}{2}F$, $F + \frac{1}{3}F$, and $F + \frac{1}{4}F$. From figure 13(*a*), we see that when $f = F + \frac{1}{2}F$ two different modes of mixing-layer growth exist. That is, when β is close to $\frac{1}{2}\pi$, the mixing layer grows immediately downstream of the origin. We call this Mode I. On the other hand, when β is close to 0, the growth of the mixing layer is delayed. We call this Mode II. The difference in the mixing-layer growth between Modes I and II is clearly seen in figures 14(*a*) and 14(*b*). In the figures, the double-frequency forced case of $f = F + \frac{1}{2}F$ is compared to the momentum thickness distributions of the

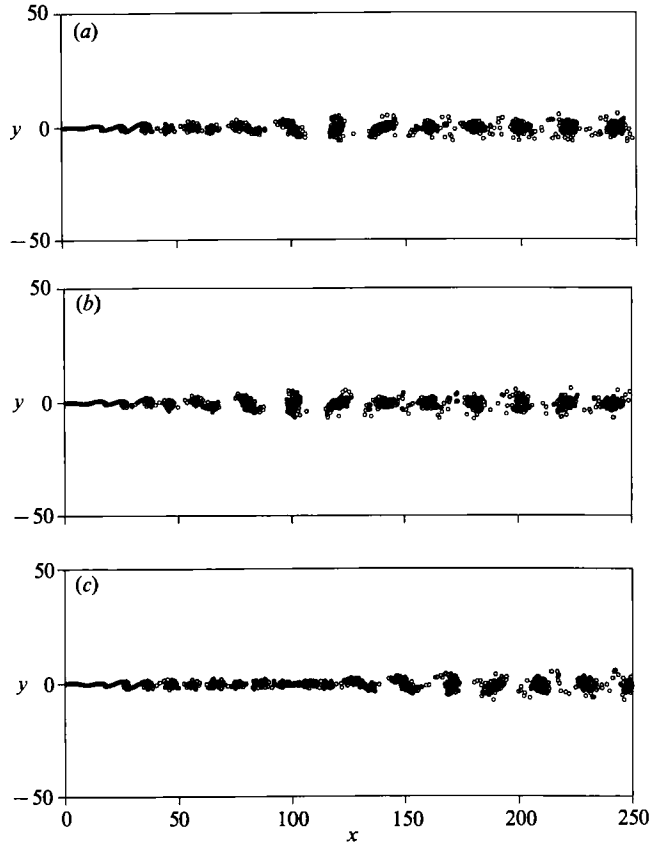

FIGURE 15. Effect of phase shift on vortex merging. Case I: $f = F + \frac{1}{2}F$, $t = 1400$. (*a*) $\beta = \frac{1}{8}\pi$ (Mode I), (*b*) $\beta = \frac{1}{2}\pi$ (Mode I), (*c*) $\beta = 0$ (Mode II).

unforced mixing layer and the single-frequency forced mixing layers with $f = F$ and $f = \frac{1}{2}F$. In Mode I, the mixing layer grows immediately after the roll-up of vortices ($40 \leqslant x \leqslant 100$), and the momentum thickness distribution in this region is close to the single-frequency forced case with $f = \frac{1}{2}F$, suggesting that the flow in this region is governed by the first subharmonic frequency. On the other hand, in Mode II the growth of the mixing layer is suppressed after the roll-up of vortices ($40 \leqslant x \leqslant 100$) and is close to that of the single-frequency forced mixing layer with $f = F$, suggesting that the mixing layer is governed by the fundamental frequency in this region. Downstream of this region the mixing layer grows and the momentum thickness approaches the value of the single-frequency forced case with $f = \frac{1}{2}F$. Instantaneous plots of discrete vortices for $f = F + \frac{1}{2}F$ are shown in figure 15. The flows shown in figures 15(*a*) and 15(*b*) are close to Mode I, while figure 15(*c*) is for Mode II. As we can see, in Mode I merging of every two vortices occurs immediately after the roll-up of vortices, leading to the rapid growth of the mixing layer in this region. On the other hand, in Mode II vortex merging is delayed, leading the suppression of mixing-layer growth after the roll-up of vortices. Figure 13(*a*) indicates that on increasing β from 0 to $\frac{1}{2}\pi$ the flow pattern changes from Mode II to Mode I. The change from Mode II to Mode I is rapid and at $\beta = \frac{1}{8}\pi$ the flow is close to Mode I, as seen from figures 13(*a*) and 15(*a*). Thus, we may say that when the amplitude ratio a is equal to 1.0, Mode II appears in a narrow region of β around 0.

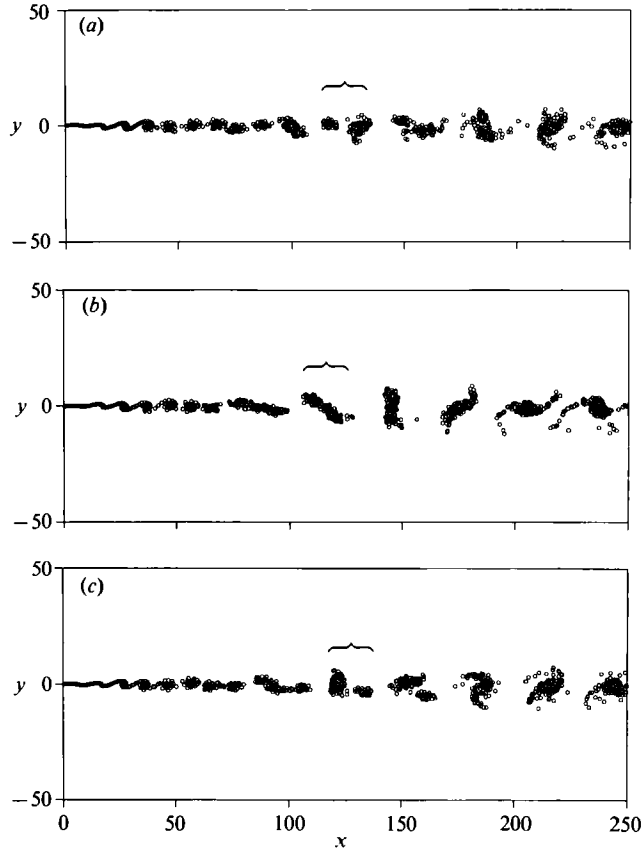

FIGURE 16. Effect of phase shift on vortex merging. Case I: $f = F + \frac{1}{3}F$, $t = 1400$. (a) $\beta = \frac{1}{6}\pi$, (b) $\beta = \frac{1}{2}\pi$, (c) $\beta = \frac{1}{3}\pi$.

(The effect of the amplitude ratio on the appearance of Modes I and II will be discussed in §3.2.3.) In both Modes I and II, the momentum thickness ratio before and after merging of every two vortices is about 2, as seen from figures 13(a) and 14.

Jacobs & Pullin (1989) observed in their numerical study of a time-developing shear layer that, when the fundamental frequency is combined with its first subharmonic, either vortex pairing or vortex tearing occurs depending on whether the phase shift is 0 or $\frac{1}{2}\pi$. A similar dependence of the nature of vortex interaction had been observed by Patnaik *et al.* (1976) and Riley & Metcalfe (1980). Our results for a spatially growing mixing layer also show two patterns of vortex interaction and Mode I may correspond to the vortex pairing mode. However, Mode II does not necessarily correspond to the vortex tearing mode. As will be seen later in figure 23 in §3.2.3, vortex tearing (or shredding) is observed over a narrow range of β around 0 with a sufficiently large amplitude ratio.

When $f = F + \frac{1}{3}F$, sets of three vortices merge regularly, as we noted before. Depending on β, three different patterns of vortex merging are observed. Figure 16 shows instantaneous plots of discrete vortices for (a) $\beta = \frac{1}{6}\pi$, (b) $\beta = \frac{1}{2}\pi$, and (c) $\beta = \frac{1}{3}\pi$. For (a), two vortices downstream merge first. Then this new vortex merges with a third upstream one. For (b), three vortices merge simultaneously. For (c), two vortices upstream merge first. Then this new vortex merges with a third downstream one. Consistent with the dependency of the vortex merging pattern on β, figure 13(b) shows that the momentum thickness distributions are also dependent on β. Among

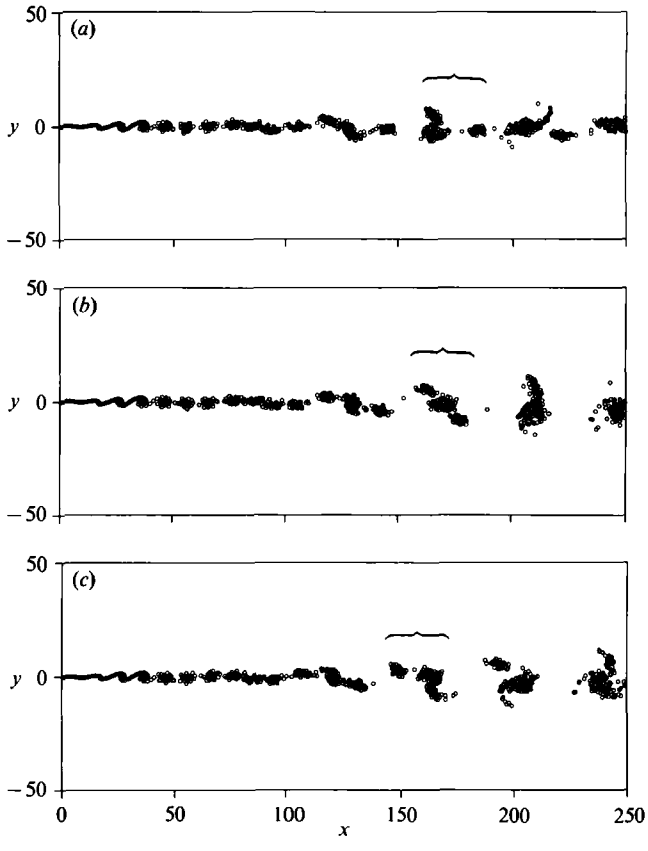

FIGURE 17. Effect of phase shift on vortex merging. Case I: $f = F + \frac{1}{4}F$, $t = 1400$, (*a*) $\beta = \frac{1}{8}\pi$ (Type A), (*b*) $\beta = \frac{1}{4}\pi$ (Type B), (*c*) $\beta = \frac{3}{8}\pi$ (Type C).

the three patterns, simultaneous merging of three vortices is unstable to irregular disturbances. For example, when forcing was reset suddenly at a particular moment ($t = 200$, actually), that is, when the forcing disturbances given by (7) are suddenly changed, while keeping the parameters A_1, A_2, f_1, f_2 and β unchanged, to those given by

$$y_f = A_1 \sin(2\pi f_1 \tilde{t}) + A_2 \sin(2\pi f_2 \tilde{t} + \beta), \tag{11}$$

where $\tilde{t} = t - t_1$ and $t_1 = 200$, the subsequent vortex merging pattern of the mixing layer with $\beta = \frac{1}{2}\pi$ was changed from initial simultaneous merging shown in figure 16(*b*) to the pattern shown in figure 16(*a*). (The other two patterns were stable to the irregular disturbances, and each pattern of vortex merging was unchanged.) Therefore, when $f = F + \frac{1}{3}F$, simultaneous merging of three vortices may be observed only at certain times in actual flows, consistent with an experimental observation by Ho & Huang (1982) that in most tests of their mode III mixing layer two vortices merge first and the new vortex merges with a third one. The patterns of three vortices merging shown in figures 16(*a*) and 16(*c*) have been also observed by Matsui & Okude (1983) in the wake of a circular cylinder which was forced by sound with a forcing frequency nearly equal to one-third of the fundamental frequency. Among the three patterns of vortex merging, Jacobs & Pullin (1989) observed simultaneous merging of three vortices only in their contour-dynamics simulation of a time-developing flow.

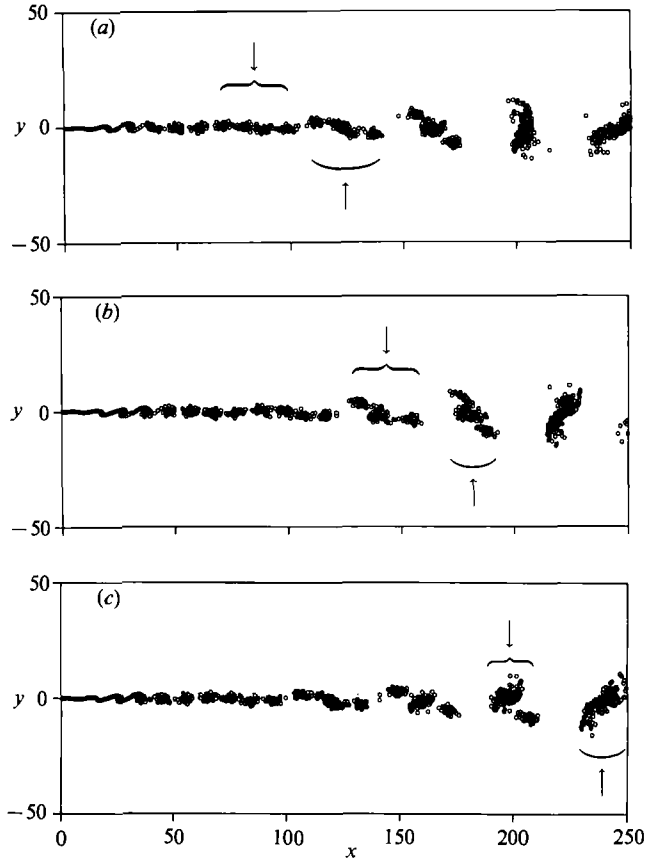

FIGURE 18. Merging of every four vortices when forcing was reset at $t = 200$. Case I: $f = F + \frac{1}{4}F$, $\beta = 0$. (*a*) $t = 1412$, (*b*) $t = 1430$, (*c*) $t = 1448$.

When $f = F + \frac{1}{4}F$, the relative phase range over which β varies is $\frac{1}{2}\pi$. Depending on β, vortex merging patterns change and we observed the following three patterns. Type A: Among each set of four vortices, the inner two merge into a pair first. Then this pair merges with the third, most upstream vortex. Then, this new vortex merges with the fourth, most downstream vortex. Type B: the inner two merge first. Then, this new vortex merges with the other two simultaneously. Type C: as in Type A, but, this time the pair merges with the third, most downstream vortex, then this new vortex merges with the fourth, most upstream vortex. Typical examples are presented in figure 17. When $\beta = \frac{1}{8}\pi$, both Types A and C appear though only Type A can be seen in figure 17(*a*). Irrespective of the Type, the merging of the vortex produced by first three vortices with the fourth one inhibited over $150 \leqslant x \leqslant 250$, and as a result the growth of the mixing layer when $\beta = \frac{1}{8}\pi$ is suppressed in this region, as seen from the momentum thickness distribution in figure 13(*c*). When $\beta = \frac{1}{4}\pi$, Type B appears, as seen from figure 17(*b*). When $\beta = \frac{3}{8}\pi$, Type C appears, as shown in figure 17(*c*). This pattern of vortex merging is observed also when $\beta = 0$ (see figure 10). The vortex merging pattern is not always stable. For example, when forcing was reset suddenly at $t = 200$ in the same way as mentioned above (equation (11)), the pattern of vortex merging when $\beta = 0$ changed from Type C shown in figure 10 to a mixed pattern of Types A (↓) and B (↑), as seen in figure 18, though Type A was observed only at times.

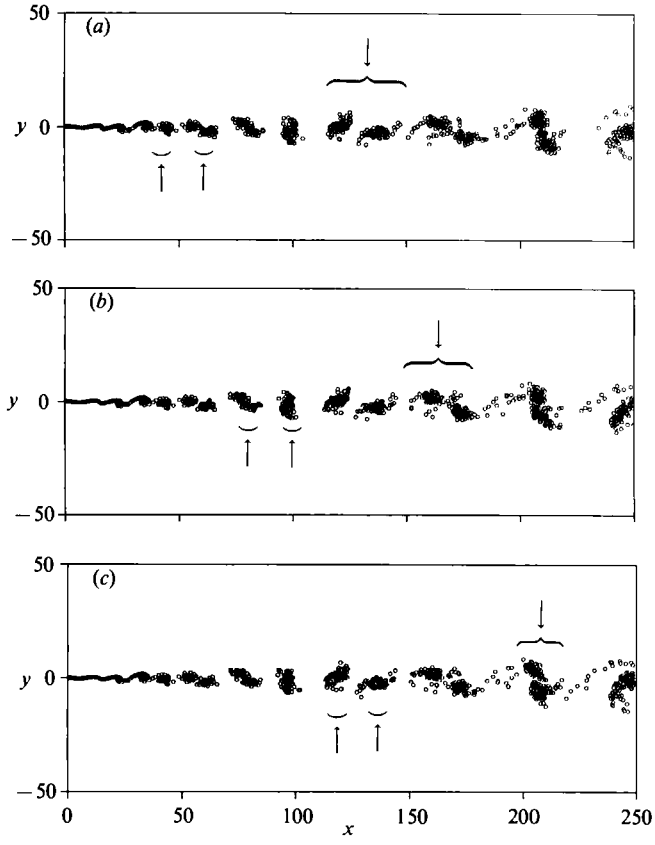

FIGURE 19. Two-stage merging of every four vortices in a triple-frequency forced mixing layer. $f = F + \frac{1}{2}F + \frac{1}{4}F$. $\beta_1 = \frac{1}{2}\pi$, $\beta_2 = \frac{1}{2}\pi$. (*a*) $t = 1412$, (*b*) $t = 1424$, (*c*) $t = 1436$.

Ho & Huang (1982) observed, in their mode IV mixing layer where every four vortices merge, that two vortices usually merge into a pair and two pairs then form a single structure. This pattern of two-stage vortex merging may lead an additional plateau (and thus three saturation regions) of momentum thickness (figure 26 in Ho & Huang). They also observed at times that four vortices merge simultaneously. These patterns of vortex merging were not observed in the present study. The pattern of two-stage vortex merging mentioned above is observed in a triple-frequency forced mixing layer with $f = F + \frac{1}{2}F + \frac{1}{4}F$, and for reference instantaneous plots of discrete vortices and momentum thickness distributions are shown in figures 19 and 20 respectively (Inoue 1991).

3.2.3. *Effect of forcing amplitude*

The effect of forcing amplitude on flow structures is examined by varying the amplitude ratio $a\,(\equiv A_2/A_1)$ with a fixed value of $A_1\,(=0.5U_c\,\delta t)$. With a larger value of a, the effects of a subharmonic frequency become larger while with a smaller value of a, the effects of the fundamental frequency become larger. The effect of a on the momentum thickness distribution when $f = F + \frac{1}{2}F$ are presented in figure 21. Figure 21 (*a*) is for $\beta = \frac{1}{2}\pi$, while figure 21 (*b*) is for $\beta = 0$. With a small value of $a = 0.05$, the mixing layer is in Mode II irrespective of β, because the effect of the fundamental frequency F is prevailing in the region immediately after the roll-up of vortices. For

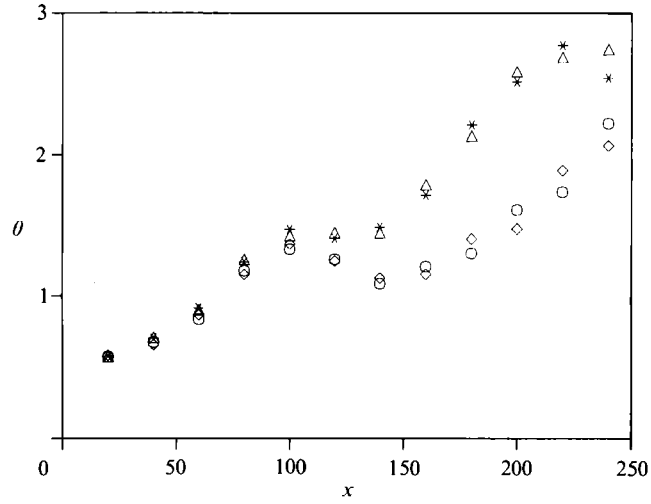

FIGURE 20. Momentum thickness distributions for a triple-frequency forcing. $f = F + \frac{1}{2}F + \frac{1}{4}F$, $\beta_1 = \frac{1}{2}\pi$, *, $\beta_2 = -\frac{1}{2}\pi$; ○, $\beta_2 = 0$; △, $\beta_2 = \frac{1}{2}\pi$; ◇, $\beta_2 = \pi$.

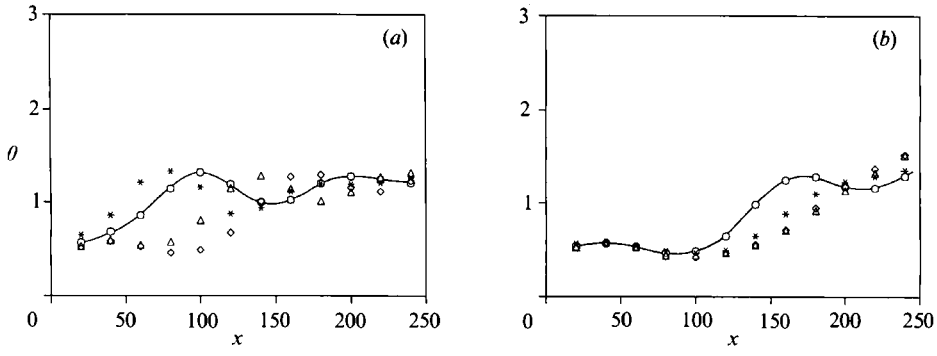

FIGURE 21. Effect of amplitude ratio on momentum thickness distributions. $f = F + \frac{1}{2}F$. (a) $\beta = \frac{1}{2}\pi$, (b) $\beta = 0$. *, $a = 2$; -○-, $a = 1$; △, $a = 0.2$; ◇. $a = 0.05$.

$\beta = \frac{1}{8}\pi$, $\frac{1}{4}\pi$, $\frac{3}{8}\pi$ and $\frac{1}{2}\pi$ the streamwise location at which every two vortices start to merge regularly moves upstream with increasing a, and vortex merging pattern changes from Mode II at $a = 0.05$ to Mode I, as seen from figure 21 (a) and also from figure 22, where the dependence of the vortex merging pattern on a for $\beta = \frac{1}{2}\pi$ is presented as an example. On the other hand, when β is close to 0 the mixing layer stays in Mode II irrespective of a, as seen in figure 21 (b). Instantaneous plots of vortices shown in figure 23 suggest that, when the amplitude ratio is sufficiently large, a larger vortex (indicated by ↓ in figure 23) and a smaller vortex (↑) appear alternately in the region where the vortex merging is inhibited ($x \leqslant 100$ in figure 23). This alternate appearance of larger and smaller vortices may be considered as evidence of vortex tearing (or shredding). Thus, our result indicates that vortex tearing occurs in a narrow region of β around zero with a sufficiently large amplitude ratio.

The dependence of the momentum thickness distribution on a when $f = F + \frac{1}{3}F$ is presented in figure 24 for $\beta = 0$ and $\frac{1}{2}\pi$, for an example. When $f = F + \frac{1}{3}F$, with increasing a, the streamwise location at which every three vortices start to merge moves upstream, irrespective of β. The vortex merging patterns for $\beta = \frac{1}{2}\pi$ are

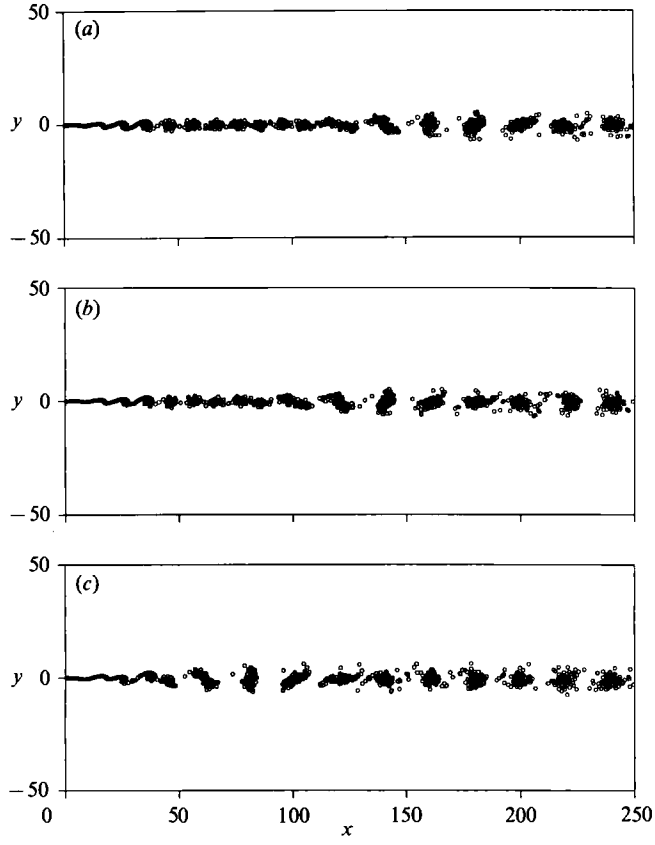

FIGURE 22. Effect of amplitude ratio on vortex merging. $f = F + \frac{1}{2}F$, $\beta = \frac{1}{2}\pi$, $t = 1400$. (*a*) $a = 0.05$, (*b*) $a = 0.2$, (*c*) $a = 2$.

presented in figure 25, as an example. When a is small, among the three patterns shown in figure 16 two patterns, but not the simultaneous vortex merging, are observed irrespective of β. With increasing a, the effect of the subharmonic frequency starts to prevail and one of the three patterns of vortex merging appears, depending on β.

The effects of the amplitude ratio a on the momentum thickness distribution and on the vortex merging pattern when $f = F + \frac{1}{4}F$ are similar to those when $f = F + \frac{1}{3}F$. The streamwise station where every four vortices start to merge moves upstream with increasing a, irrespective of β. Instantaneous plots of discrete vortices for $\beta = \frac{1}{6}\pi$ are presented in figure 26 as an example. A new type of vortex merging pattern (Type D) was observed when $a = 2.0$ with $\beta = \frac{1}{8}\pi$. That is, among each four vortices, downstream three vortices merge simultaneously, first. Then, this new vortex merges with the fourth, most upstream vortex (see figure 26*c*).

3.3. *Double-frequency forced flows (Case II)*

Momentum thickness distributions for Case II are presented in figure 27 for $\Delta F = \frac{1}{4}F$, $\frac{1}{6}F$ and $\frac{1}{8}F$. In Case II, as in Case I, the fundamental frequency dominates the roll-up process. The rolled-up vortices tend to merge regularly, but this time the number of merging vortices depends on ΔF, and for small values of ΔF sets of m vortices merge when $\Delta F = F/2m$; that is, every four vortices merge regularly when $\Delta F = \frac{1}{8}F$, every

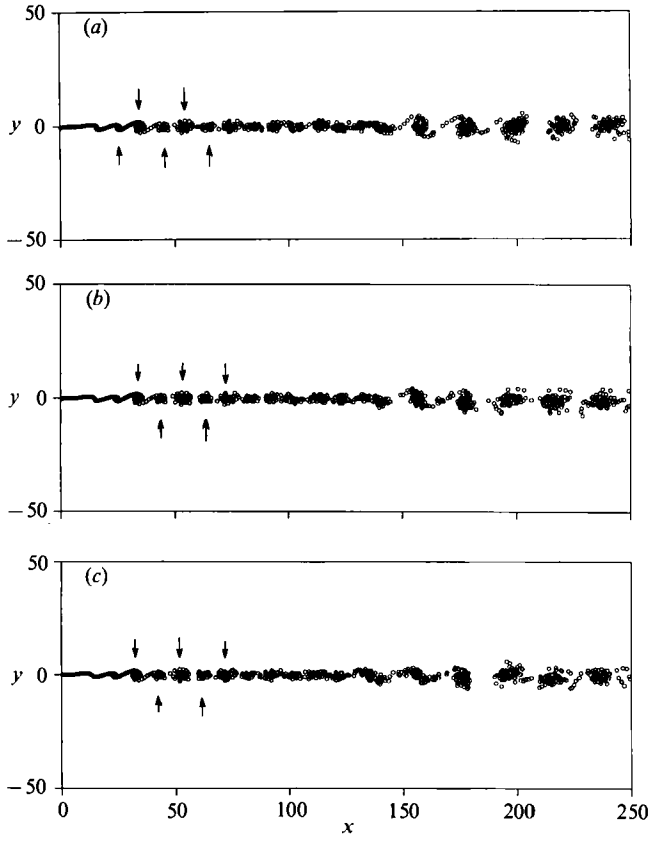

FIGURE 23. Vortex tearing mode in Mode II. $f = \frac{1}{2}F + F$, $\beta = 0$, $a = 2.0$. (*a*) $t = 1412$, (*b*) $t = 1424$, (*c*) $t = 1436$.

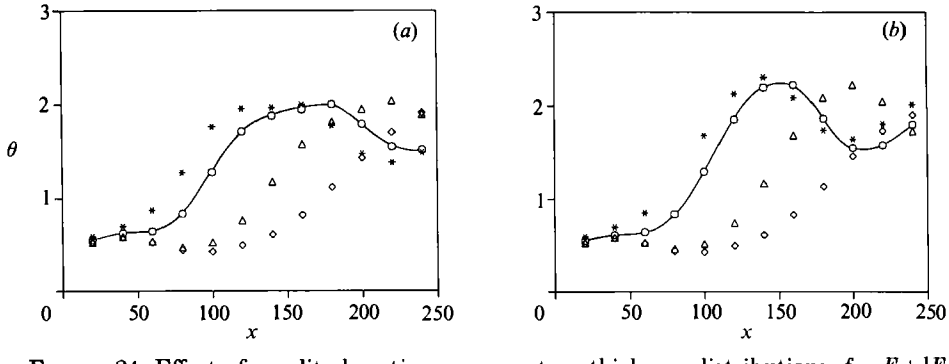

FIGURE 24. Effect of amplitude ratio on momentum thickness distributions. $f = F + \frac{1}{3}F$. (*a*) $\beta = 0$, (*b*) $\beta = \frac{1}{2}\pi$. *, $a = 2$; –○–, $a = 1$; △, $a = 0.2$; ◇, $a = 0.05$.

three vortices when $\Delta F = \frac{1}{6}F$. Time developments of forced mixing layers when $\Delta F = \frac{1}{8}F$ and $\frac{1}{6}F$ are presented in figures 28 and 29, respectively. The mechanism of regular merging of sets of m vortices when $\Delta F = F/2m$ may be explained by the nonlinear interaction of the two forcing frequencies; that is, by combining $f_1 (= F + \Delta F)$ and $f_2 (= F - \Delta F)$, new frequencies $2F$ and $2\Delta F (= F/m)$ may be produced through the nonlinear interaction. Thus, the combination of the new

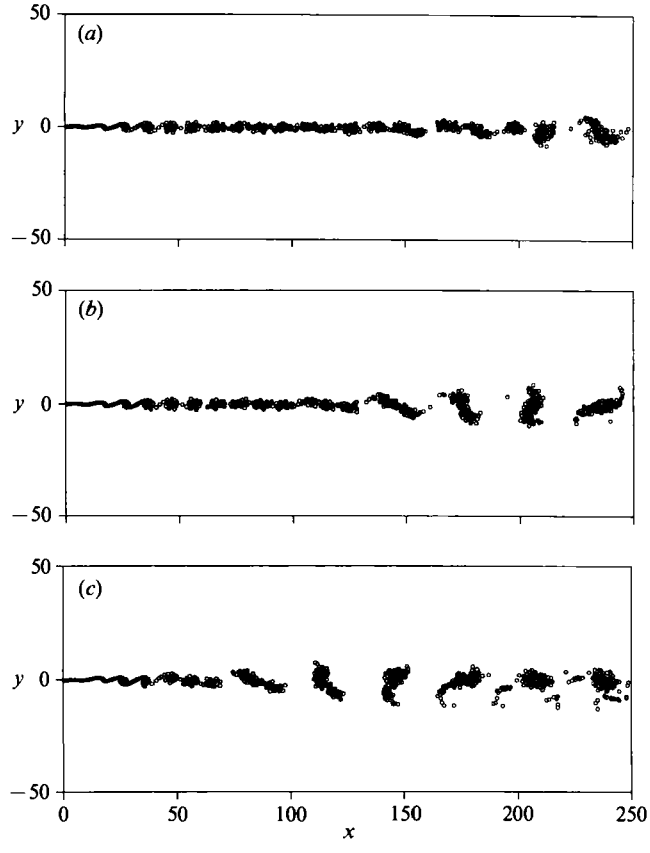

FIGURE 25. Effect of amplitude ratio on vortex merging. $f = F + \frac{1}{3}F$, $\beta = \frac{1}{2}\pi$, $t = 1400$. (*a*) $a = 0.05$, (*b*) $a = 0.2$, (*c*) $a = 2$.

frequency $2\Delta F\,(=F/m)$ with the fundamental frequency F may lead the regular merging of m vortices in a manner similar to Case I where the forcing frequency is given by $f = F + F/m$.

For the larger value of ΔF equal to $\frac{1}{4}F$, however, the number of merging vortices was not two. Instead, as seen in figure 30, two vortices merging and three vortices merging occur alternately, and these two new vortices then merge into a single structure; thus eventually every five vortices merge. In figure 30, downward arrows indicate three vortices merging while upward arrows indicate two vortices merging. Though at present we have no definite explanation for the mechanism of five vortices merging when $\Delta F = \frac{1}{4}F$, the result seems to suggest that there is a further way to control the number of merging vortices and consequently the growth of a mixing layer. As seen from figure 27, rapid growth of a mixing layer produced by multiple-vortex merging is followed by a saturation region where vortex merging is inhibited.

The dependence of momentum thickness distributions on the relative phase shift β in Case II is presented in figure 31 for $\Delta F = \frac{1}{8}F$, $\frac{1}{6}F$, and $\frac{1}{4}F$. When $\Delta F = \frac{1}{8}F$, every four vortices merge regularly as occurred for $f = F + \frac{1}{4}F$ in Case I. The phase range over which β varies may be $\frac{1}{2}\pi$ in this case, as for $f = F + \frac{1}{4}F$ in Case I. In fact, the differences in the momentum thickness distributions among the four cases of $\beta = 0$, $\pm\frac{1}{2}\pi$ and π were negligible. As seen from figure 31 (*a*), the momentum thickness distribution depends on β. The effect of β on vortex merging is presented in figure 32.

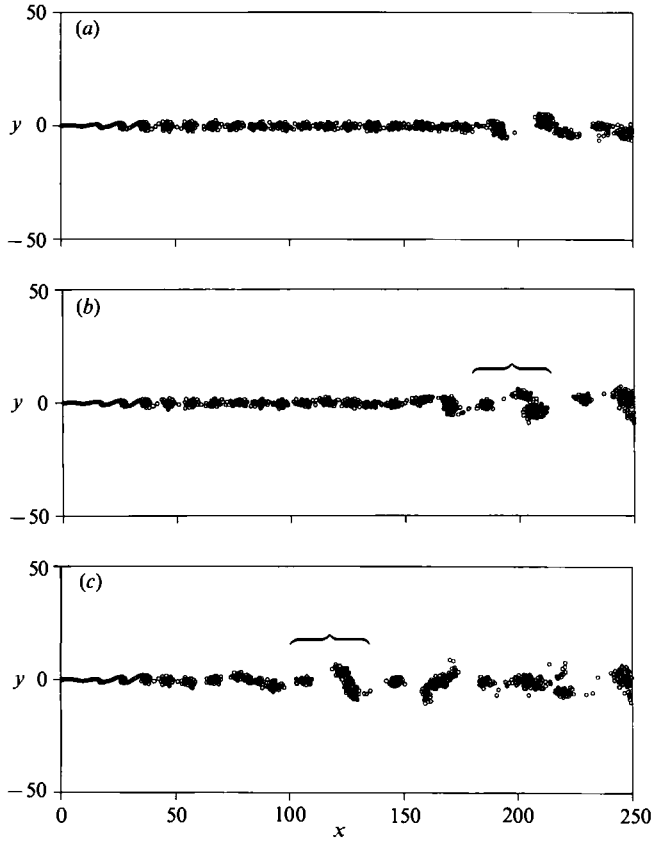

FIGURE 26. Effect of amplitude ratio on vortex merging $f = F + \frac{1}{4}F$, $\beta = \frac{1}{8}\pi$. (a) $a = 0.05$, (b) $a = 0.2$, (c) $a = 2$.

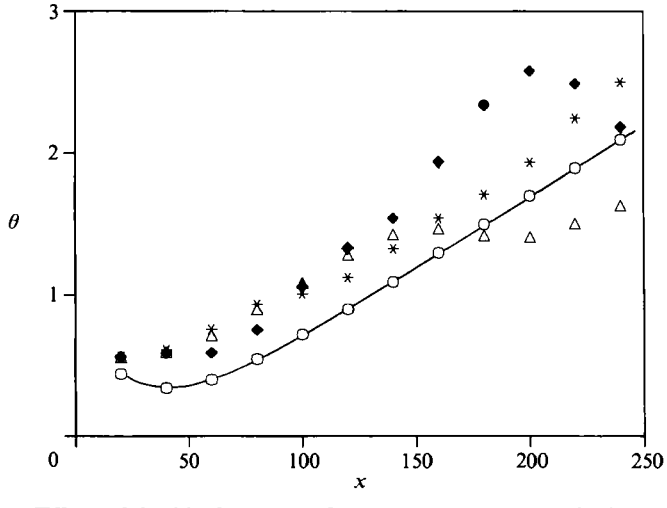

FIGURE 27. Effect of double-frequency forcing on momentum thickness distributions. Case II: $\beta = \frac{1}{2}\pi$, $a = 1$, $r = 0.6$. –○–, $f = 0$; *, $\Delta F = \frac{1}{4}F$; △, $\Delta F = \frac{1}{6}F$; ◆, $\Delta F = \frac{1}{8}F$.

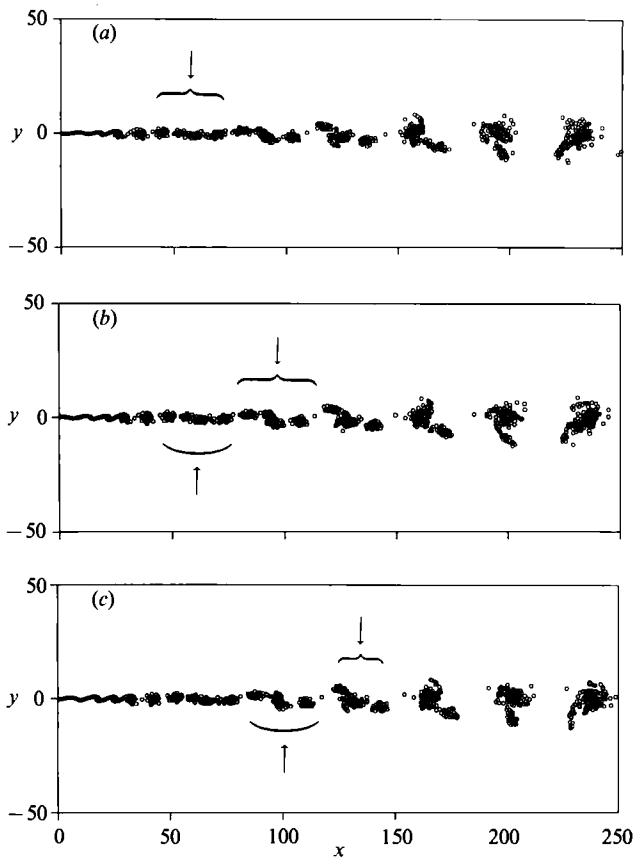

FIGURE 28. Merging of every four vortices. Case II: $\Delta F = \frac{1}{8}F$, $\beta = 0$, $a = 1$. (*a*) $t = 1412$, (*b*) $t = 1424$, (*c*) $t = 1436$.

As was seen in figure 28, when $\beta = 0$, the vortex merging pattern is Type A defined in §3.2.2. When $\beta = \frac{3}{8}\pi$, as seen from figure 32(*c*), the pattern is of Type B. When $\beta = \frac{1}{8}\pi$ and $\frac{1}{4}\pi$, a new type was observed. That is, as seen from figures 32(*a*) and 32(*b*), among the four vortices upstream, two merge into a pair first. Then this pair emerges with the third downstream vortex, and finally this new vortex merges with the fourth, most downstream vortex. We call Type E. By comparing with the case of $\beta = \frac{1}{8}\pi$ in figures 31(*a*) and 32(*a*), we can see that when $\beta = \frac{1}{4}\pi$ the vortex merging is delayed and thus the growth of the mixing layer is suppressed in the region ($x \geqslant 100$) after the initial merging of two upstream vortices. From these results, we may say that the effect of β is profound in this case $\Delta F = \frac{1}{8}F$ as it was for $f = F + \frac{1}{4}F$ in Case I.

When $\Delta F = \frac{1}{6}F$, as for $f = F + \frac{1}{3}F$ in Case I, every three vortices merge regularly. However, as seen from figure 31(*b*), the momentum thickness distributions in this case show no appreciable difference among all the values of β examined, in strong contrast to $f = F + \frac{1}{3}F$ in Case I (Figure 13*b*). The dependency on β of the appearance of the three different patterns of vortex merging found in Case I (figure 16) does not hold in Case II; that is, the three patterns can be seen irrespective of β, as seen in figure 29. In accordance with the previous note in Case I, however, simultaneous merging of three vortices shown in figure 16(*b*) was observed only at times in Case II.

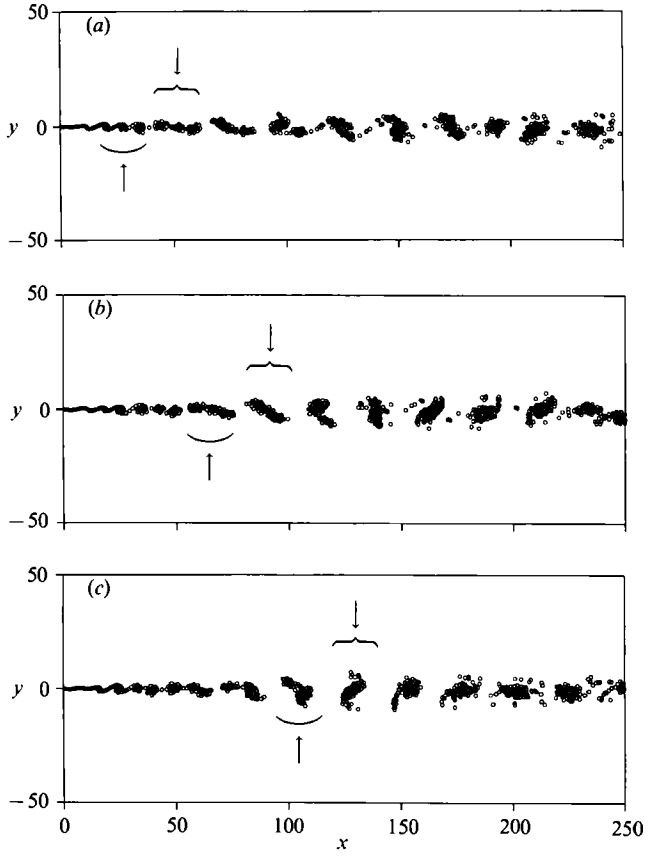

FIGURE 29. Merging of every three vortices. Case II: $\Delta F = \frac{1}{6}F$, $\beta = \frac{1}{6}\pi$, $a = 1$. (*a*) $t = 1406$, (*b*) $t = 1418$, (*c*) $t = 1430$.

In the case of $\Delta F = \frac{1}{4}F$ as well as $\Delta F = \frac{1}{6}F$, no appreciable effect of β on momentum thickness distributions (figure 31*c*) nor on vortex merging pattern was observed. Therefore, in this study β had no effect only when $\Delta F = \frac{1}{6}F$ and $\frac{1}{4}F$, both in Case II. As noted in the introduction, Wygnanski & Petersen (1987) claim that calculations based on the temporal evolution of a shear flow overemphasize the importance of the initial phase shift because temporal waves are non-dispersive. Our calculation considers a spatially growing flow, and the above results partly support Wygnanski & Petersen. Further accumulation of data is necessary.

4. Summary and concluding remarks

The effects of double-frequency forcing on the growth of spatially growing mixing layers were examined using a two-dimensional vortex method. Forcing frequencies were prescribed in two different manners (Cases I and II). The results for Case I showed that the number of merging vortices can be controlled by a combination of a fundamental frequency with its subharmonics; sets of two vortices merge regularly when $f = F + \frac{1}{2}F$, every three vortices merge when $f = F + \frac{1}{3}F$, and every four merge when $f = F + \frac{1}{4}F$. It was also found that the phase shift between two forcing frequencies has a profound effect on the process of vortex merging and thus on the growth of a mixing layer. That is, when $f = F + \frac{1}{2}F$ the growth of a mixing layer was

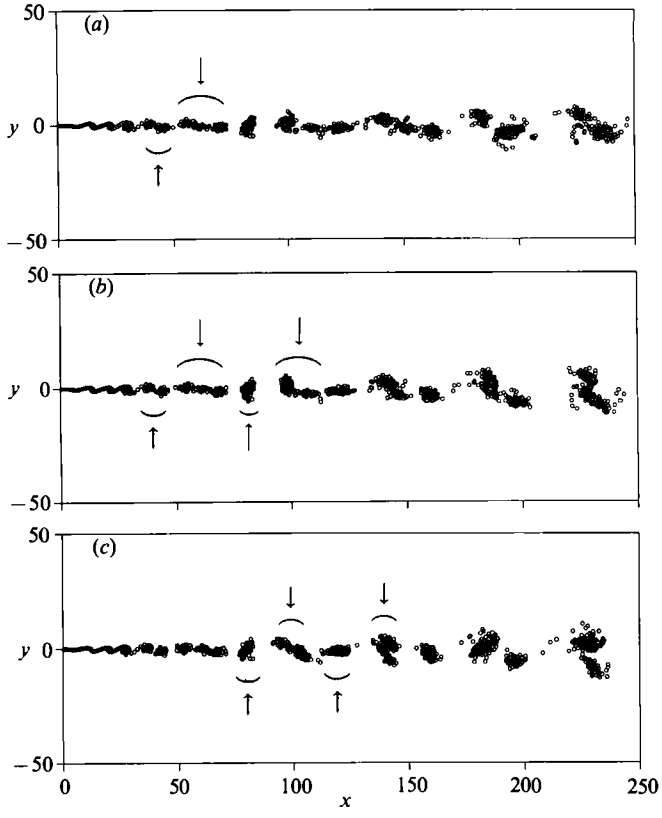

FIGURE 30. Alternate merging of every two and every three vortices. Case II: $\Delta F = \frac{1}{4}F$, $\beta = 0$, $a = 1$. (*a*) $t = 1412$, (*b*) $t = 1424$, (*c*) $t = 1436$.

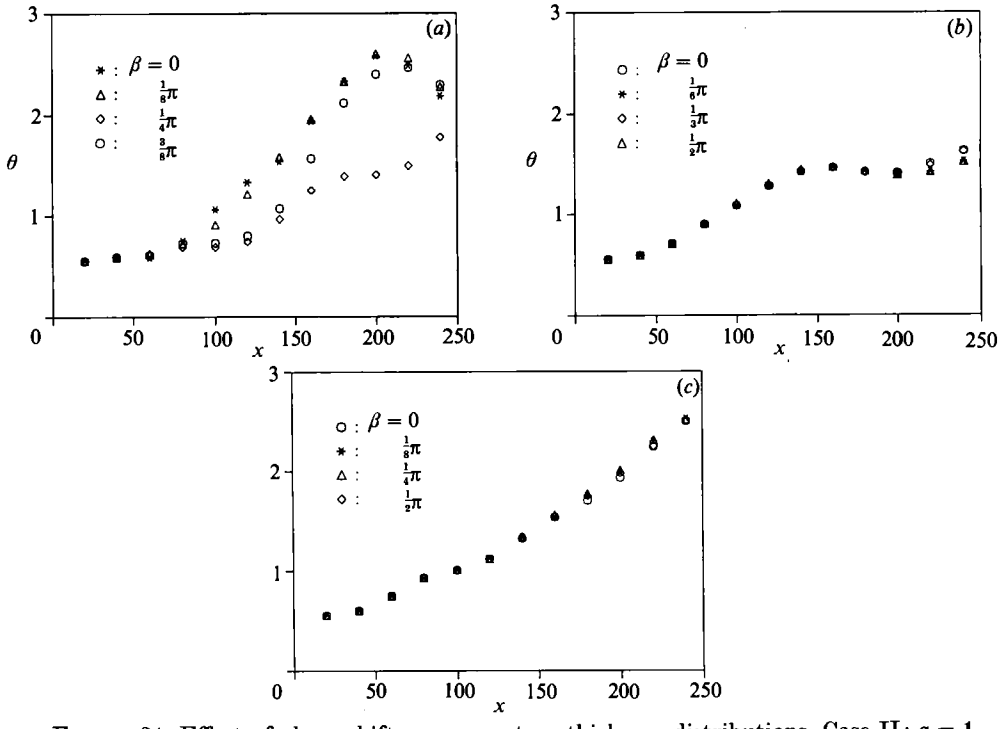

FIGURE 31. Effect of phase shift on momentum thickness distributions. Case II: $a = 1$. (*a*) $\Delta F = \frac{1}{6}F$, (*b*) $\Delta F = \frac{1}{6}F$, (*c*) $\Delta F = \frac{1}{4}F$.

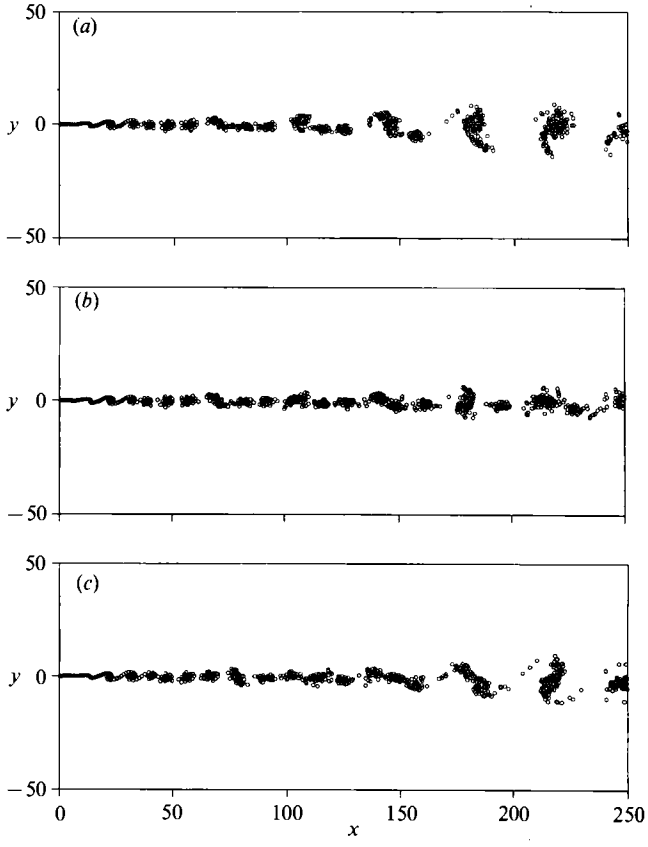

FIGURE 32. Effect of phase shift on vortex merging. Case II: $\Delta F = \frac{1}{8}F$, $a = 1$, $t = 1400$. (a) $\beta = \frac{1}{8}\pi$, (b) $\beta = \frac{1}{4}\pi$, (c) $\beta = \frac{3}{8}\pi$.

enhanced immediately downstream of the origin for all the values of β examined, except for $\beta = 0$ where it was delayed. When $f = F + \frac{1}{3}F$ and also $F + \frac{1}{4}F$, different patterns of vortex merging were observed, depending on β, and the momentum thickness distributions also varied. The effect of forcing amplitude was also found to be important. With a small value of amplitude ratio a, the effect of the fundamental frequency is larger and the growth of the mixing layer is suppressed in the region immediately after the roll-up of vortices. With increasing a, the effect of a subharmonic frequency becomes larger and the streamwise location at which multiple-vortex merging starts to occur moves upstream, in general, leading the rapid growth of the mixing layer. However, when $f = \frac{1}{2}F + F$ with β close to 0, the mixing layer growth was not enhanced even with a sufficiently large value of a. In this case, a larger vortex and a smaller vortex appeared alternately, indicating that the flow is in the vortex tearing (or shredding) mode.

The results for Case II indicate that the number of merging vortices can also be controlled by prescribing the two frequencies such that $f_1 = F + \Delta F$ and $f_2 = F - \Delta F$, where ΔF was set equal to F/n ($n = 4, 6, 8$). For small values of ΔF (and thus large values of n), it was found that sets of m vortices merge when $n = 2m$; that is, every three vortices merge when $n = 6$, and every four when $n = 8$. This relation has been confirmed to hold at least up to $n = 12$, when every six vortices merge. For a larger value of $\Delta F = \frac{1}{4}F$, however, the above relation did not hold. Instead, two-vortex

merging and three-vortex merging occurred alternately, suggesting a further way to control the growth of a mixing layer. In Case II the effect of phase shift was observed only for $\Delta F = \frac{1}{8}F$: no appreciable effect of β was seen for $\Delta F = \frac{1}{6}F$ and $\frac{1}{4}F$.

The author expresses his sincere thanks to Professor H. Sato, Institute of Flow Research, and Professor M. Kiya, Faculty of Engineering, Hokkaido University, for their valuable advice and fruitful discussions. Thanks are also given to Mr S. Onuma, Institute of Fluid Science, Tohoku University, for his assistance in this study. The computation in this work was done by the use of CRAY Y-MP at Institute of Fluid Science, Tohoku University.

REFERENCES

BUELL, J. C. & HUERRE, P. 1988 Inflow/outflow boundary conditions and global dynamics of spatial mixing layers. In *Proc. 1988 Summer Program of NASA/Stanford Center for Turbulence Research* (*Rep.* CTR-S 88), pp. 19–27.

HO, C. M. & HUANG, L. S. 1982 Subharmonics and vortex merging in mixing layers. *J. Fluid Mech.* **119**, 443–473.

HO, C. M. & HUERRE, P. 1984 Perturbed free shear layers. *Ann. Rev. Fluid Mech.* **16**, 365–424.

HUSSAIN, F. & HUSAIN, H. S. 1989 Subharmonic resonance in a free shear layer. In *Proc. 4th Asian Cong. Fluid Mech.*, Vol. II, pp. A288–A291.

INOUE, O. 1989 Artificial control of turbulent mixing layers. In *Structures of Turbulence and Drag Reduction, IUTAM Symp., Zurich, Switzerland* (ed. A. Gyr), pp. 145–152. Springer.

INOUE, O. 1991 Effects of multiple-frequency forcing on spatially-growing mixing layers. In *Proc. 8th Symp. Turbulent Shear Flow*, vol. 1, pp. 3.4.1–3.4.6.

INOUE, O. & LEONARD, A. 1986 Vortex simulation of forced mixing layers. *NASA TM* 88235.

INOUE, O. & LEONARD, A. 1987*a* Vortex simulation of forced/unforced mixing layers. *AIAA Paper* 87-0288.

INOUE, O. & LEONARD, A. 1987*b* Vortex simulation of forced/unforced mixing layers. *AIAA J.* **25**, 1417–1418.

JACOBS, P. A. & PULLIN, D. I. 1989 Multiple-contour-dynamic simulation of eddy scales in the plane shear layer. *J. Fluid Mech.* **199**, 89–124.

KELLY, R. E. 1967 On the stability of an inviscid shear layer which is periodic in space and time. *J. Fluid Mech.* **7**, 657–689.

MANSOUR, N. N., HUSSAIN, F. & BUELL, J. C. 1988 Subharmonic resonance in a mixing layer. In *Proc. 1988 Summer Program of NASA/Stanford Center for Turbulence Research* (*Rep.* CTR-S 88), pp. 57–68.

MATSUI, T. & OKUDE, M. 1983 Formation of the secondary vortex street in the wake of a circular cylinder. In *Proc. IUTAM Symp. on Structure of Complex Turbulent Shear Flows* (ed. R. Dumas & L. Fulachier), pp. 156–164. Springer.

MEHTA, R. D., INOUE, O., KING, L. S. & BELL, J. H. 1987 Comparison of experimental and computational techniques for plane mixing layers. *Phys. Fluids* **30**, 2054–2062.

OSTER, D. & WYGNANSKI, I. 1982 The forced mixing layer between parallel streams. *J. Fluid Mech.* **123**, 91–130.

PATNAIK, P. C., SHERMAN, F. S. & CORCOS, G. M. 1976 A numerical simulation of Kelvin–Helmholtz waves of finite amplitude. *J. Fluid Mech.* **73**, 215–240.

RILEY, J. J. & METCALFE, R. W. 1980 Direct numerical simulation of a perturbed turbulent mixing layer. *AIAA Paper* 80-0274.

WEISBROT, I. & WYGNANSKI, I. 1988 On coherent structures in a highly excited mixing layer. *J. Fluid Mech.* **195**, 137–159.

WYGNANSKI, I. J. & PETERSEN, R. A. 1987 Coherent motion in excited free shear flows. *AIAA J.* **25**, 201–213.

WYGNANSKI, I. & WEISBROT, I. 1988 On the pairing process in an excited plane turbulent mixing layer. *J. Fluid Mech.* **195**, 161–173.

ZAMAN, K. B. Q. M. & HUSSAIN, A. K. M. F. 1980 Vortex pairing in a circular jet under controlled excitation. Part 1. General jet response. *J. Fluid Mech.* **101**, 449–491.